Microscopic two-component multistep direct theory for continuum nuclear reactions

A. J. Koning
Netherlands Energy Research Foundation ECN, BU–Nuclear Energy, P.O. Box 1, 1755 ZG Petten, The Netherlands

M. B. Chadwick
University of California, Theoretical Division, Los Alamos National Laboratory, Los Alamos, New Mexico 87545
(Received 23 December 1996)

We present a multistep direct reaction theory for analyzing nucleon-induced reactions to the continuum for incident energies up to 200 MeV. Two principal advances in multistep direct theory are studied. (1) A microscopical approach is given for calculating distorted-wave Born approximation (DWBA) transitions to the continuum, where transitions to all accessible $1p1h$ shell model states are explicitly determined. These states, obtained from a simple noninteracting Nilsson model, are assumed to be spread according to Gaussian distributions. In this approach, therefore, state densities are not used. We also provide a link with more conventional methods that utilize particle-hole state densities, and present a more accurate technique for sampling the DWBA strength. (2) A two-component formulation of multistep direct reactions is given, where neutron and proton excitations are explicitly accounted for in the evolution of the reaction, for all orders of scattering. We show that the attractive convolution structure for multistep processes persists within a two-component formalism, and conveniently automatically generates the many reaction pathways that can occur in the Feshbach-Kerman-Koonin expansion of the multistep cross section when neutron and proton excitations are followed. This formalism is particularly important for the simultaneous analyses of neutron and proton emission spectra. The multistep direct theory is applied, along with theories for multistep compound, compound, and collective reactions, to analyze experimental emission spectra for a range of targets and energies. Particular attention is paid to a complete and comprehensive analysis of all important decay channels and reaction mechanisms. We show that the theory correctly accounts for measured neutron and proton emission angle-integrated spectra, as well as angular distributions. Additionally, we note that these microscopic and two-component developments facilitate more fundamental studies into effective nucleon-nucleon interactions in multistep calculations. [S0556-2813(97)01108-4]

PACS number(s): 24.60.Gv, 24.60.Dr, 25.40.Ep, 24.50.+g

I. INTRODUCTION

The preequilibrium nuclear reaction mechanism comprises the bridge between fast, direct processes, and slow compound processes, and accounts for the high-energy tails in emission spectra and the smooth forward-peaked angular distributions. In recent years quantum mechanical theories have been developed to describe these mechanisms [1–3] and the advent of fast computers has enabled numerical computations of these cross sections. After pioneering calculations by Tamura *et al.* [4] and Bonetti and co-workers [5,6], several independent and more sophisticated computer codes for both multistep direct (MSD) and multistep compound (MSC) processes have emerged, enabling a better insight into the contributions of each reaction mechanism to the spectrum. Although some controversies regarding the underlying quantum statistics in multistep reactions still exist (such as causality issues in the MSD theory of Feshbach, Kerman, and Koonin [7,8]), quantum mechanical preequilibrium theories tend to account for experimental angle-integrated emission spectra with an accuracy comparable to that found in the semiclassical models, and with a higher accuracy for angular distributions, competing with the phenomenological experiment-based systematics of Kalbach [9].

In cases where direct reactions account for scattering to low-lying discrete states, it is natural to expect that such directlike mechanisms persist in the continuum. An extension of discrete direct reactions to this continuum part of the spectrum is then provided by the multistep direct (MSD) model (where in the term ''MSD'' the important one-step direct cross section is included). When a reaction proceeds by the MSD mechanism, it is imagined that at least one particle is in the continuum throughout the process and that at each subsequent step of the reaction a new particle-hole pair is created. After one or a few collisions, the continuum particle is emitted in a direction that still has retained some coupling to the initial direction and is therefore forward peaked. The main difference with conventional direct reaction theories is the high density of final and intermediate states, which necessitates statistical postulates in the direct reaction formalism so that the analysis of these processes remains tractable. The three most prominent statistical MSD theories are those of Feshbach, Kerman, and Koonin (FKK) [8], Tamura, Udagawa, and Lenske [4] (TUL), and Nishioka, Weidenmüller, and Yoshida (NWY) [10]. A comparison of both the theoretical [11] and practical [12] aspects of these models revealed that the FKK model, derived using a statistical assumption called leading-particle statistics, is computationally the most attractive model because of its convolution structure. Furthermore, it was concluded that, despite considerable theoretical differences concerning their quantum-statistical assumptions, the three models appear to have essentially equivalent predictive powers with respect to double-differential cross sections when they are calculated

on the same consistent basis. The relative simplicity of the FKK equations is reflected by the popularity of this model in nuclear reaction analyses.

Previous analyses of MSD reactions have largely ignored complications which arise due to the possibility of exciting both neutron and proton excitations during the multistep reaction (some recent works have made some studies in this area, resulting in correction factors for one-step scattering [13]). In this paper we present a formalism for calculating MSD cross sections in a fully two-component theory where all possible neutron and proton particle-hole excitations are explicitly followed, for all orders of scattering. While this may at first seem to be a formidable task, especially for multistep processes where the many possible reaction pathways becomes large in a two-component formalism, we show that this is not so—a rather simple generalization of the FKK convolution expression automatically generates these pathways. Such considerations are particularly relevant when simultaneously analyzing both neutron and proton emission spectra, which is always important since these processes represent competing decay channels.

In this paper we also study a new, and fully microscopic, method for calculating MSD cross sections which does not make use of particle-hole state densities but instead directly calculates cross sections for all possible particle-hole excitations (again including an exact book-keeping of the neutron/proton type of the particle and hole at all stages of the reaction) determined from a simple noninteracting shell model. This is in contrast to all previous numerical implementations of the FKK theory which sample only a small number of such states to estimate the distorted-wave Born approximation (DWBA) strength, and utilize simple analytical formulas for the partial state density, based on the equidistant spacing model. The development of this microscopic method has been possible due to the advent of fast workstations. In the process of developing this approach we have also arrived at a more accurate technique for sampling the DWBA cross sections within the more conventional approach which utilizes state densities. In this paper we will argue that our approach removes several uncertainties related to MSD reactions and that it may serve as a starting point for analyses that involve more sophisticated nuclear structure models.

In Sec. II we present the multistep direct formalism in a two-component form, both for the completely microscopic approach and the approach that utilizes partial state densities. In Sec. III we describe our use of the shell model and the associated DWBA calculations for the particle-hole states. Section IV contains an outline of the smoothing and averaging procedure that leads to the computation of the multistep direct equations. In Sec. V we compare our method with other MSD approaches that have been used in the past. Section VI describes the complementary nuclear reaction models (direct reactions to discrete states, multistep compound, compound and multiple MSD emission) that are included in this work. In Sec. VII the results of MINGUS, the code system that contains all the nuclear models presented in this paper, are compared with experimental data and discussed. Finally, we give our conclusions and recommendations for future refinements in Sec. VIII.

II. THEORY

The double-differential MSD cross section to the continuum is an incoherent sum of a one-step term and multistep terms,

$$\frac{d^2\sigma_{j\leftarrow i}(E,\Omega\leftarrow E_0,\Omega_0)}{d\Omega dE}=\sum_{n=1}^{\infty}\frac{d^2\sigma_{j\leftarrow i}^{(n)}(E,\Omega\leftarrow E,\Omega_0)}{d\Omega dE}, \tag{2.1}$$

where E_0,Ω_0,i, and E,Ω,j are the energy, solid angle, and type of the incident and outgoing nucleon, respectively. In this section, we will show using the methodology and notation of Refs. [3,11], how the different terms of the MSD cross section can be rewritten into a form that enables excited neutrons and protons to be distinguished and followed throughout all scattering stages. The various terms of Eq. (2.1) can be obtained by extending standard distorted-wave theory to the continuum which leads to cross section distributions of first and higher orders. Then, using an average over the outgoing (and, for the higher steps, intermediate) energy combined with statistical assumptions one obtains an expression for the continuum cross section for each step. Products of distorted wave matrix elements of different order cancel out, which leads to the incoherent sum (2.1). Since the two-component extension of the derivation of Refs. [3,11] is straightforward, we will directly present the various terms of the expansion (2.1) here. In this paper, we will restrict ourselves to reactions involving incident and outgoing nucleons.

A. The one-step cross section

In all MSD models, the continuum one-step direct cross section is given by the same expression. It is a weighted sum over squared DWBA matrix elements that describe transitions to particle-hole states μ. In a two-component form, it is given by

$$\frac{d^2\sigma_{j\leftarrow i}^{(1)}(E,\Omega\leftarrow E_0,\Omega_0)}{d\Omega dE}$$
$$=\frac{m^2}{(2\pi\hbar^2)^2}\frac{k}{k_0}\sum_{\mu}\hat{\rho}_{\mu}(p_\pi,h_\pi,p_\nu,h_\nu,E_x)|\langle\chi_j^{(-)}(E,\Omega)|$$
$$\times\langle\mu(p_\pi,h_\pi,p_\nu,h_\nu)|\mathcal{V}|0\rangle|\chi_i^{(+)}(E_0,\Omega_0)\rangle|^2, \tag{2.2}$$

where k and k_0 are the final and initial momentum and $E_x=E_0-E+Q$ is the excitation energy with Q the reaction Q value. The distorted waves χ are eigenfunctions of the Schrödinger equation with an optical potential. They satisfy, together with their bi-orthogonally conjugated counterparts $\hat{\chi}$, the orthonormality and completeness relations

$$\langle\chi^{(+)}(\mathbf{k})|\hat{\chi}^{(+)}(\mathbf{k}')\rangle=(2\pi)^3\delta(\mathbf{k}-\mathbf{k}'),$$
$$\int\frac{d\mathbf{k}}{(2\pi)^3}|\chi^{(+)}(\mathbf{k})\rangle\langle\hat{\chi}^{(+)}(\mathbf{k})|=1, \tag{2.3}$$

and analogous relations hold for $\hat{\chi}^{(-)}$. The different excited model states are characterized by a set of numbers $(p_\pi,h_\pi,p_\nu,h_\nu)$ of proton (neutron) particles $p_\pi(p_\nu)$ and holes $h_\pi(h_\nu)$. In Eq. (2.2) we explicitly designate which type

of particle and hole is involved in the reaction, e.g., (1,0,0,1) designates a proton-particle, neutron-hole excitation. Depending on the type of incident and outgoing nucleon, the indices can take the values (1,1,0,0), (0,0,1,1), (1,0,0,1), and (0,1,1,0) in a one-step direct reaction. In order not to overburden the notation, we assume it obvious that charge conservation restricts the summation over μ in Eq. (2.2) to the subset of particle-hole states that can be excited by the reaction under consideration. The effective nucleon-nucleon interaction $\mathcal{V}$ manifests itself in $\mathcal{V}_{\pi\pi}$, $\mathcal{V}_{\pi\nu}$ $(=\mathcal{V}_{\nu\pi})$, and $\mathcal{V}_{\nu\nu}$ components. The contribution of each particle-hole state to the continuum is determined by the $1p1h$ distribution $\hat{\rho}_\mu$. In the derivation of Eq. (2.2) it is shown that this distribution is given by

$$\hat{\rho}_\mu(p_\pi,h_\pi,p_\nu,h_\nu,E_x)=\sum_f \overline{|a_\mu^f|^2\delta(E_f-E_x)}, \quad (2.4)$$

where the bar denotes the average over the final nuclear states f. Here, a_μ^f are distribution amplitudes of $1p1h$ states which may generally be dependent on the nucleon type of the particle and hole. Each real nuclear state f, with energy E_f, consist of a linear combination of particle-hole states, the particular combination being given by $a_{m\mu}^f$,

$$|f\rangle=\sum_{m\mu} a_{m\mu}^f|m\mu\rangle, \quad (2.5)$$

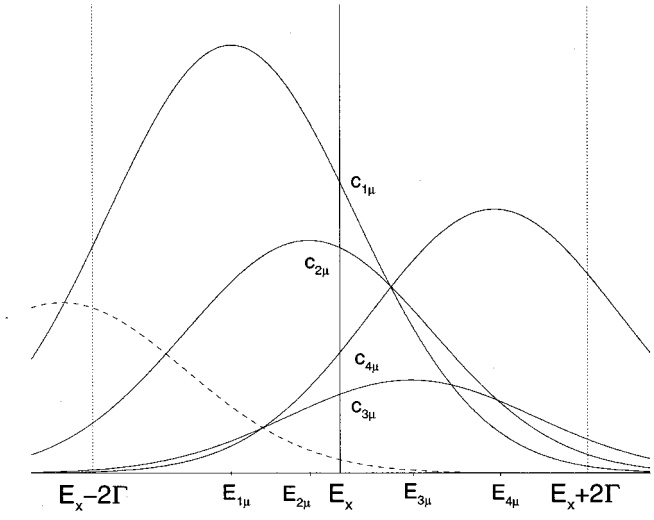

FIG. 1. Distribution of the $1p1h$ states over the real states (Sec. II A). The excitation energy (corresponding with an outgoing energy E) is represented by the solid vertical line. Typically, DWBA cross sections for $1p1h$ states that lie within $\pm 2\Gamma$ of E_x are taken into account, where Γ is the width of each $1p1h$ distribution and the intersections $c_\mu=G(E_\mu,E_x)$ are the contributions to the MSD cross section (Sec. IV). In this strongly simplified case, with only four $1p1h$ states with the same J, the total contribution to E_x is given by $S_J(E_x)=c_{1\mu}+c_{2\mu}+c_{3\mu}+c_{4\mu}$, see Eq. (4.5), which is the normalization factor for a state density-based approach (Sec. IV B). The strength of each $1p1h$ state is reflected by the height of the Gaussian. The state represented by the dashed Gaussian lies outside the boundaries (the two dotted lines) and does not contribute at E_x in our approximation.

where m denotes the exciton class ($mpmh$ states). Since $\mathcal{V}$ is assumed to be of a two-body nature, only the $1p1h$ combinations of Eq. (2.5) survive in the one-step expression (2.2) and accordingly we have dropped the index $m=1$ for simplicity. The physical interpretation of $\hat{\rho}_\mu$ is that around each particle-hole state a probability distribution is given, its width being a measure for the magnitude of the residual interaction within the nucleus. Then, the contribution of each particle-hole state to a real nuclear state is represented by the value of $\hat{\rho}_\mu$ at the energy E_x of the real state, see Fig. 1. When $\hat{\rho}_\mu$ is in addition arithmetically averaged over the particle-hole states μ, the resulting $\hat{\rho}_{1p1h}$ is often referred to as a true $1p1h$ state density [14].

As we consider incident and outgoing nucleons in this paper, it is instructive to explicitly give expressions for both charge exchange and inelastic scattering. In a (p,n) reaction, the excited particle-hole pair is necessarily of the (1,0,0,1) type and the effective interaction is $\mathcal{V}_{\pi\nu}$. Hence, Eq. (2.2) becomes

$$\frac{d^2\sigma_{\nu\leftarrow\pi}^{(1)}(E,\Omega\leftarrow E_0,\Omega_0)}{d\Omega\,dE} = \frac{m^2}{(2\pi\hbar^2)^2}\frac{k}{k_0}\sum_\mu \hat{\rho}_\mu(1,0,0,1,E_x)|\langle\chi_\nu^{(-)}(E,\Omega)| \times\langle\mu(1,0,0,1)|\mathcal{V}_{\pi\nu}|0\rangle|\chi_\pi^{(+)}(E_0,\Omega_0)\rangle|^2, \quad (2.6)$$

and the corresponding diagram is displayed in Fig. 2. An analogous equation applies for an (n,p) reaction where the configuration is (0,1,1,0). In a (p,p') reaction, both (1,1,0,0)

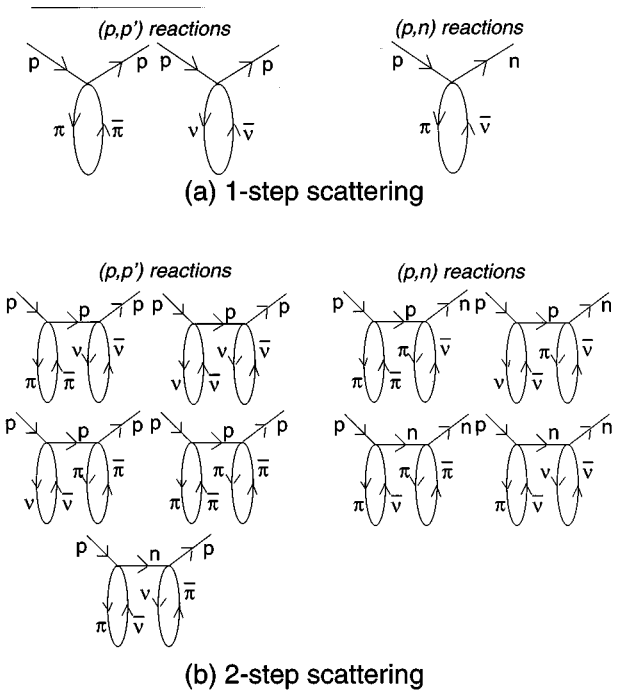

FIG. 2. Particle-hole excitations within a two-component formalism: (a) one-step (p,p') and (p,n) scattering, see Eqs. (2.6)–(2.7), (b) two-step (p,p') and (p,n) scattering, see Eqs. (2.10)-(2.11). The symbols with a bar designate the holes.

and (0,0,1,1) pairs can be excited and both $\mathcal{V}_{\pi\pi}$ and $\mathcal{V}_{\pi\nu}$ are involved, see Fig. 2. The cross section is a sum over both possibilities:

$$\frac{d^2\sigma^{(1)}_{\pi\leftarrow\pi}(E,\Omega\leftarrow E_0,\Omega_0)}{d\Omega dE} = \frac{m^2}{(2\pi\hbar^2)^2}\frac{k}{k_0}\sum_{\mu}\,[\hat{\rho}_{\mu}(1,1,0,0,E_x)|\langle\chi^{(-)}_{\pi}(E,\Omega)| \times\langle\mu(1,1,0,0)|\mathcal{V}_{\pi\pi}|0\rangle|\chi^{(+)}_{\pi}(E_0,\Omega_0)\rangle|^2 + \hat{\rho}_{\mu}(0,0,1,1,E_x)|\langle\chi^{(-)}_{\pi}(E,\Omega)|\langle\mu(0,0,1,1)|\mathcal{V}_{\pi\nu}|0\rangle \times|\chi^{(+)}_{\pi}(E_0,\Omega_0)\rangle|^2], \tag{2.7}$$

and an analogous equation applies for an (n,n') reaction. Equations (2.6) and (2.7) indicate that all DWBA matrix elements should be calculated using the appropriate component of the effective interaction and a form factor that involves only the specific types of nucleons of the excited particle-hole state.

The use of the $1p1h$ distributions $\hat{\rho}_{\mu}$ is a general feature of *any* MSD model and is not a feature differentiating various MSD models. It was first applied by Tamura *et al.* [4]. However, their distorted-wave calculation involved macroscopic form factors instead of separate form factors for each particle-hole state and also did not distinguish between excited neutrons and protons. We improve both aspects in the present work. The fully microscopic one-step direct calculation of the TUL model, of which preliminary results were shown in Ref. [4], is automatically included here. The original FKK paper [8] was not explicit on the type of level density to be used. Until now, practitioners have replaced $\hat{\rho}_{1p1h}$ by particle-hole densities based on the equidistant spacing model, such as that of Williams [15], for FKK analyses because of their simplicity. This may give the false impression that the use of analytical state density formulas characterizes the FKK model, and the distributions $\hat{\rho}_{\mu}$ the TUL model. We stress here that the FKK model has only one basic characteristic: the well-known convolution structure of the multistep terms, which distinguishes it from other MSD models that involve the full second (and higher) order distorted wave matrix elements. The actual description of the nuclear structure in the continuum should be considered as a separate issue.

B. The multistep cross section

The derivation of the two-step FKK cross section from the continuum distorted-wave theory is by no means trivial and has led to a certain amount of controversy [3,16,17]. Applying leading-particle statistics directly on the two-step cross section distribution [11] yields a continuum two-step direct formula with a modified DWBA cross section, which contains a distorted wave $|\chi^{(+)}\rangle$ in the incident channel and a $\langle\chi^{(+)}|$ in the outgoing channel. To overcome this problem, Feshbach [18] has argued that an extra energy averaging is required *before* the application of any statistical postulates. His argument is that without such an average interference effects, which would normally cancel out in the single-channel case, are incorrectly transferred to the statistical multistep expression yielding an unphysical enhancement of the multistep terms. In mathematical terms, the extra energy averaging leads to a rotation of S-matrix poles that allows the replacement of the conjugated outgoing distorted wave $\hat{\chi}^{(+)}$ by an energy-averaged incoming distorted wave $\overline{\chi^{(-)}}$. This enables the continuum two-step cross section to be expressed as a product of two normal DWBA cross sections. In this paper we adopt the expression with normal DWBA matrix elements.

The complete derivation that leads to the two-step cross section is given in [3]. When we repeat this while distinguishing between neutrons and protons, there appears an extra summation over t_1, indicating both types of intermediate nucleons,

$$\frac{d^2\sigma^{(2)}_{j\leftarrow i}(E,\Omega\leftarrow E_0,\Omega_0)}{d\Omega dE} = \frac{2m^5}{(2\pi)^8\hbar^{10}}\frac{k}{k_0}2\pi^2\sum_{t_1=\pi,\nu}\sum_{\mu}\sum_{\mu'}\int d\Omega_1\int dE_1E_1\hat{\rho}_{\mu'}(p_{\pi},h_{\pi},p_{\nu},h_{\nu},E''_x) \times\hat{\rho}_{\mu}(p_{\pi},h_{\pi},p_{\nu},h_{\nu},E'_x)|\langle\overline{\chi^{(-)}_{j}}(E,\Omega)|\langle\mu'(p_{\pi},h_{\pi},p_{\nu},h_{\nu})|\mathcal{V}|0\rangle|\overline{\chi^{(+)}_{t_1}}(E_1,\Omega_1)\rangle|^2 \times|\langle\overline{\chi^{(-)}_{t_1}}(E_1,\Omega_1)|\langle\mu(p_{\pi},h_{\pi},p_{\nu},h_{\nu})|\mathcal{V}|0\rangle|\overline{\chi^{(+)}_{i}}(E_0,\Omega_0)\rangle|^2, \tag{2.8}$$

where E_1,Ω_1 are the intermediate energy and solid angle, respectively, and $E'_x=E_0-E_1+Q_1$ and $E''_x=E_1-E+Q_2$, with Q_1 and Q_2 the reaction Q values at each stage.[1] The extra summation over t_1 automatically appears in the two-component derivation of Eq. (2.8): the intermediate scattering states involving protons and neutrons are just two subsets of all possible intermediate states.

The sum over t_1 in Eq. (2.8) indicates that the number of possible scattering terms is larger compared to the one-component approach. Nevertheless, the attractive convolution structure remains present in the two-component approach. Indeed, combining Eq. (2.2) and Eq. (2.8) gives

[1]We understand that using Q values is inconsistent with the intermediate nucleon being localized within the nucleus. These inconsistencies are not expected to introduce significant errors.

$$\frac{d^2\sigma^{(2)}_{j\leftarrow i}(E,\Omega\leftarrow E_0,\Omega_0)}{d\Omega dE}=\frac{m}{4\pi^2\hbar^2}\sum_{t_1=\pi,\nu}\int d\Omega_1\int dE_1E_1\frac{d^2\sigma^{(1)}_{j\leftarrow t_1}(E,\Omega\leftarrow E_1,\Omega_1)}{d\Omega dE}\frac{d^2\sigma^{(1)}_{t_1\leftarrow i}(E_1,\Omega_1\leftarrow E_0,\Omega_0)}{d\Omega_1 dE_1}. \quad (2.9)$$

Here we again give the explicit equations for charge exchange and inelastic scattering. For a (p,n) reaction, the two-step cross section consists of four different two-step sequences. The different diagrams are shown in Fig. 2. The explicit expression for Eq. (2.8), which is automatically generated by substituting Eqs. (2.6) and (2.7) in Eq. (2.9), is

$$\begin{aligned}\frac{d^2\sigma^{(2)}_{\nu\leftarrow\pi}(E,\Omega\leftarrow E_0,\Omega_0)}{d\Omega dE}=&\frac{2m^5}{(2\pi)^8\hbar^{10}}\frac{k}{k_0}2\pi^2\sum_{\mu}\sum_{\mu'}\int d\Omega_1\int dE_1E_1\\
&\times\{[\hat\rho_{\mu'}(0,0,1,1,E''_x)|\langle\overline{\chi^{(-)}_{\nu}}(E,\Omega)|\langle\mu'(0,0,1,1)|\mathcal{V}_{\nu\nu}|0\rangle|\overline{\chi^{(+)}_{\nu}}(E_1,\Omega_1)\rangle|^2\\
&+\hat\rho_{\mu'}(1,1,0,0,E''_x)|\langle\overline{\chi^{(-)}_{\nu}}(E,\Omega)|\langle\mu'(1,1,0,0)|\mathcal{V}_{\nu\pi}|0\rangle|\overline{\chi^{(+)}_{\nu}}(E_1,\Omega_1)\rangle|^2]\hat\rho_{\mu}(1,0,0,1,E'_x)\\
&\times|\langle\overline{\chi^{(-)}_{\nu}}(E_1,\Omega_1)|\langle\mu(1,0,0,1)|\mathcal{V}_{\pi\nu}|0\rangle|\overline{\chi^{(+)}_{\pi}}(E_0,\Omega_0)\rangle|^2+\hat\rho_{\mu'}(1,0,0,1,E''_x)\\
&\times|\langle\overline{\chi^{(-)}_{\nu}}(E,\Omega)|\langle\mu'(1,0,0,1)|\mathcal{V}_{\pi\nu}|0\rangle|\overline{\chi^{(+)}_{\pi}}(E_1,\Omega_1)\rangle|^2[\hat\rho_{\mu}(0,0,1,1,E'_x)\\
&\times|\langle\overline{\chi^{(-)}_{\pi}}(E_1,\Omega_1)|\langle\mu(0,0,1,1)|\mathcal{V}_{\pi\nu}|0\rangle|\overline{\chi^{(+)}_{\pi}}(E_0,\Omega_0)\rangle|^2+\hat\rho_{\mu}(1,1,0,0,E'_x)\\
&\times|\langle\overline{\chi^{(-)}_{\pi}}(E_1,\Omega_1)|\langle\mu(1,1,0,0)|\mathcal{V}_{\pi\pi}|0\rangle|\overline{\chi^{(+)}_{\pi}}(E_0,\Omega_0)\rangle|^2]\}. \quad (2.10)\end{aligned}$$

Similarly, for inelastic scattering, there are five terms that contribute to the two-step cross section, see Fig. 2. The (p,p') two-step cross section reads

$$\begin{aligned}\frac{d^2\sigma^{(2)}_{\pi\leftarrow\pi}(E,\Omega\leftarrow E_0,\Omega_0)}{d\Omega dE}=&\frac{2m^5}{(2\pi)^8\hbar^{10}}\frac{k}{k_0}2\pi^2\sum_{\mu}\sum_{\mu'}\int d\Omega_1\int dE_1E_1\\
&\times\{[\hat\rho_{\mu'}(0,0,1,1,E''_x)|\langle\overline{\chi^{(-)}_{\pi}}(E,\Omega)|\langle\mu'(0,0,1,1)|\mathcal{V}_{\pi\nu}|0\rangle|\overline{\chi^{(+)}_{\pi}}(E_1,\Omega_1)\rangle|^2\\
&+\hat\rho_{\mu'}(1,1,0,0,E''_x)|\langle\overline{\chi^{(-)}_{\pi}}(E,\Omega)|\langle\mu'(1,1,0,0)|\mathcal{V}_{\pi\pi}|0\rangle|\overline{\chi^{(+)}_{\pi}}(E_1,\Omega_1)\rangle|^2][\hat\rho_{\mu}(0,0,1,1,E'_x)\\
&\times|\langle\overline{\chi^{(-)}_{\pi}}(E_1,\Omega_1)|\langle\mu(0,0,1,1)|\mathcal{V}_{\pi\nu}|0\rangle|\overline{\chi^{(+)}_{\pi}}(E_0,\Omega_0)\rangle|^2+\hat\rho_{\mu}(1,1,0,0,E'_x)\\
&\times|\langle\overline{\chi^{(-)}_{\pi}}(E_1,\Omega_1)|\langle\mu(1,1,0,0)|\mathcal{V}_{\pi\pi}|0\rangle|\overline{\chi^{(+)}_{\pi}}(E_0,\Omega_0)\rangle|^2]+\hat\rho_{\mu'}(0,1,1,0,E''_x)\\
&\times|\langle\overline{\chi^{(-)}_{\pi}}(E,\Omega)|\langle\mu'(0,1,1,0)|\mathcal{V}_{\nu\pi}|0\rangle|\overline{\chi^{(+)}_{\nu}}(E_1,\Omega_1)\rangle|^2\hat\rho_{\mu}(1,0,0,1,E'_x)\\
&\times|\langle\overline{\chi^{(-)}_{\nu}}(E_1,\Omega_1)|\langle\mu'(1,0,0,1)|\mathcal{V}_{\pi\nu}|0\rangle|\overline{\chi^{(+)}_{\pi}}(E_0,\Omega_0)\rangle|^2\}. \quad (2.11)\end{aligned}$$

Obviously, this method can be extended to the higher steps. In general, the n-step direct cross section can be completely expressed in terms of the two-component MSD cross section of the previous stage:

$$\begin{aligned}\frac{d^2\sigma^{(n)}_{j\leftarrow i}(E,\Omega\leftarrow E_0,\Omega_0)}{d\Omega dE}=&\frac{m}{4\pi^2\hbar^2}\sum_{t_{n-1}=\pi,\nu}\int d\Omega_{n-1}\int dE_{n-1}E_{n-1}\\
&\times\frac{d^2\sigma^{(1)}_{j\leftarrow t_{n-1}}(E,\Omega\leftarrow E_{n-1},\Omega_{n-1})}{d\Omega dE}\frac{d^2\sigma^{(n-1)}_{t_{n-1}\leftarrow i}(E_{n-1},\Omega_{n-1}\leftarrow E_0,\Omega_0)}{d\Omega_1 dE_1}. \quad (2.12)\end{aligned}$$

Note that in this multistep description, we do not make the approximation that the *same* leading particle is followed throughout the scattering sequence. In line with the general MSD picture, our summation over both intermediate neutrons and protons ensures that at least one particle is in the continuum throughout the multistep process. In addition, the convolution structure of the two-component multistep formula automatically generates all possible cross terms involving various types of excited particle-hole states and leading particles. For example, for a two-step (p,n) reaction, the possible reaction sequences $(p,p')(p',n)$ and $(p,n')(n',n)$ are both taken into account, including the associated component of $\mathcal{V}$ and the type of excited particle-hole pair at each stage of the reaction. Each separate one-step term of the multistep expansion gives one (for charge exchange) or two (for inelastic scattering) contributions. It is easy to show that the number of different terms S_n for an n-step direct cross section is given by the following recursive relations:

$$(p,n): \quad S_n = 3S_{n-1} + 1 \quad \text{with} \quad S_0 = 0,$$

$$(p,p'): \quad S_n = 3S_{n-1} - 1 \quad \text{with} \quad S_0 = 1. \qquad (2.13)$$

This aspect clearly distinguishes the two-component method from the conventional one-component method, and has consequences for the extracted strength of the effective interaction upon comparison with experimental data. We will discuss this in Sec. V. In sum, although the number of possible paths quickly increases for the higher steps, the convolution structure automatically takes care of the bookkeeping.

C. State densities

There are basically two methods to calculate the one-step and multistep direct cross sections and they will both be considered in this paper. The first method, which is new, is fully microscopic, i.e., an exact calculation of all equations we just presented. This entails calculating the DWBA cross sections for *all* particle-hole states μ that can be excited in the reaction and adopting a physically acceptable form (e.g., a Gaussian) for the $1p1h$ distribution $\hat{\rho}_\mu$. Present available computer power no longer prohibits such microscopic analyses. In the next section, we will elucidate the fully microscopic approach, which does not require state densities.

A more conventional method is to take the MSD equations and to perform an additional, arithmetic average over the particle-hole states. The one-step cross section is decomposed into terms with different total angular momenta J, and is expressed as the product of a J-dependent particle-hole state density ρ and a DWBA cross section averaged over several particle-hole states with the same J. Then, Eq. (2.2) takes on the form

$$\frac{d^2\sigma^{(1)}_{j\leftarrow i}(E,\Omega\leftarrow E_0,\Omega_0)}{d\Omega\, dE} = \sum_J \rho(p_\pi,h_\pi,p_\nu,h_\nu,J,E_x)\left\langle \frac{d\sigma_{j\leftarrow i}(E,\Omega\leftarrow E_0,\Omega_0)}{d\Omega}\right\rangle_J^{\mathcal{V}}. \qquad (2.14)$$

In particular, the (p,n) cross section (2.6) becomes

$$\frac{d^2\sigma^{(1)}_{\nu\leftarrow\pi}(E,\Omega\leftarrow E_0,\Omega_0)}{d\Omega\, dE} = \sum_J \rho(1,0,0,1,J,E_x)\left\langle \frac{d\sigma_{\nu\leftarrow\pi}(E,\Omega\leftarrow E_0,\Omega_0)}{d\Omega}\right\rangle_J^{\mathcal{V}_{\pi\nu}}. \qquad (2.15)$$

Similarly, the (p,p') cross section (2.7) reads

$$\frac{d^2\sigma^{(1)}_{\pi\leftarrow\pi}(E,\Omega\leftarrow E_0,\Omega_0)}{d\Omega\, dE} = \sum_J \rho(1,1,0,0,J,E_x)\left\langle \frac{d\sigma_{\pi\leftarrow\pi}(E,\Omega\leftarrow E_0,\Omega_0)}{d\Omega}\right\rangle_J^{\mathcal{V}_{\pi\pi}} + \sum_J \rho(0,0,1,1,J,E_x) \times \left\langle \frac{d\sigma_{\pi\leftarrow\pi}(E,\Omega\leftarrow E_0,\Omega_0)}{d\Omega}\right\rangle_J^{\mathcal{V}_{\pi\nu}}. \qquad (2.16)$$

The component of the effective interaction involved is indicated at the top of the right-hand bracket of the J-averaged DWBA cross section. The calculation of these J-averaged DWBA cross sections should involve only the types of particle-hole pairs that are specified by the associated index of ρ.

We stress here that this extra average over the particle-hole states serves only to arrive at a more tractable one-step formula with state densities and is not related to any statistical assumption involving the removal of interference effects. In a later section, we discuss how this average has been performed in previous analyses, and we present an improved method.

In principle, the state density $\rho(p_\pi,h_\pi,p_\nu,h_\nu,J,E_x)$ can be calculated exactly on the basis of some nuclear structure model. In practical calculations, it is usually replaced by an analytical expression, without taking into account residual interactions (hence the use of the symbol ρ instead of $\hat{\rho}$). In the cases that we perform MSD calculations that use state densities, we adopt the usual decomposition of the state density into a J-dependent part and an energy-dependent part:

$$\rho(p_\pi,h_\pi,p_\nu,h_\nu,J,E_x) = (2J+1)R_n(J)\,\omega(p_\pi,h_\pi,p_\nu,h_\nu,E_x). \qquad (2.17)$$

For ω, we take the Betak-Dobes state density [19] which incorporates the finite depth of the hole into the Williams equidistant spacing formula [15]. The restriction on the hole depth is crucial at high excitation energies. In addition, we take the two-component version of this formula

$$\omega(p_\pi,h_\pi,p_\nu,h_\nu,E_x) = \frac{g_\pi^{p_\pi+h_\pi} g_\nu^{p_\nu+h_\nu}}{p_\pi!h_\pi!p_\nu!h_\nu!(n-1)!} \times \sum_{k=0}^{h_\pi}\sum_{l=0}^{h_\nu}(-1)^{k+l}\binom{h_\pi}{k}\binom{h_\nu}{l} \times [E_x-\Delta-A_{\text{Pauli}}-(k+l)E_F]^{n-1} \times \Theta[E_x-\Delta-E_{PP}-(k+l)E_F], \qquad (2.18)$$

where $g_\pi = Z/13$, $g_\nu = N/13$ are the proton and neutron single-particle state density, $n = p_\pi + h_\pi + p_\nu + h_\nu$ denotes the exciton number, Δ is the pairing correction, $A_{\rm Pauli} = [p_\pi^2 + h_\pi^2 + p_\pi - 3h_\pi]/4g_\pi + [p_\nu^2 + h_\nu^2 + p_\nu - 3h_\nu]/4g_\nu$ is the Pauli correction factor, E_F is the Fermi energy (taken fixed at 38 MeV), Θ is the Heaviside step function, and $E_{PP} = [p_\pi^2 + h_\pi^2 + p_\pi - h_\pi]/2g_\pi + [p_\nu^2 + h_\nu^2 + p_\nu - h_\nu]/2g_\nu$ is the minimum energy required to excite p particles and h holes satisfying the Pauli principle.

The function $R_n(J)$ represents the spin distribution of the states in the continuum. It is given by

$$R_n(J) = \frac{2J+1}{\pi^{1/2} n^{3/2} \sigma^3} \exp\left[-\frac{(J+1/2)^2}{n\sigma^2} \right] \tag{2.19}$$

and satisfies, for any n,

$$\sum_J (2J+1) R_n(J) = 1. \tag{2.20}$$

In this paper, only the case with $n=2$ is of interest. A frequently used expression for the spin cutoff factor σ is [20]

$$\sigma^2 = 0.24 n A^{2/3}, \tag{2.21}$$

where A is the mass number of the nucleus. When we discuss the results, we will see that this form of the spin cutoff factor, and even the Wigner-type form of $R_n(J)$ itself, may not be appropriate for MSD calculations to highly excited states.

The conclusions we draw for the two-component aspects of the higher order terms remain the same when state densities are involved: Eqs. (2.15) and (2.16) can simply be inserted in the multistep term (2.12), thereby again automatically generating all neutron and proton cross terms.

III. DWBA CROSS SECTIONS

A. Nilsson model

The aforementioned formalism indicates that a significant part of an MSD analysis consists of the computation of DWBA cross sections for transitions to particle-hole states. To obtain these $1p1h$ states, single-particle states are generated with a spherical Nilsson model [21,22]. In this model, a state with oscillator quantum number N, orbital angular momentum l, and total angular momentum j ($j = l \pm s$, where s is the spin) has a single-particle energy

$$E_{Nlj} = \hbar\omega \left[N + \frac{3}{2} - v_{ll} \left(l(l+1) - \frac{1}{2} N(N+3) \right) - v_{ls} \left(ls - \frac{1}{2} \middle| s - \frac{1}{2} \right) \right], \tag{3.1}$$

where $\hbar\omega = 41 A^{-1/3}$ MeV. We have taken the coefficients v_{ll} and v_{ls} (which are different for neutrons and protons) from Seeger and Howard [23] who give these coefficients in tabular form for the first ten major shells, supplemented with a simple extrapolation to higher shells. This is sufficient to generate a set of particle-hole states for all excitation energies that are of interest in this paper.

TABLE I. Part of the particle-hole level scheme included for the 80 MeV (p,p') reaction on ^{90}Zr. All $\pi-\pi$ and $\nu-\nu$ states in the energy interval $19.5 < E_\mu < 20.5$ are given. The angle-integrated DWBA cross sections are calculated at an outgoing energy of 60 MeV, with the starting value $V_{\pi\nu} = V_{\pi\pi} = 15$ MeV and the optical model of Menet. Each individual cross section is weighted by the $(2J+1)$ degeneracy and the contribution from a Gaussian distribution, with a width of 4 MeV, centered around the real excitation energy, see Eqs. (4.2)–(4.3). The final column indicates that spin-transfer reactions are not included in our analysis due to parity conservation.

Energy (MeV)	Type	Particle	Hole	J	Cross section (mb)	Include
19.624	$\nu\nu$	$1g$ 7/2	$2s$ 1/2	3		no
				4	0.023817	yes
19.681	$\nu\nu$	$1i$13/2	$2p$ 3/2	5	0.035020	yes
				6		no
				7	0.023124	yes
				8		no
19.812	$\nu\nu$	$3p$ 1/2	$2p$ 1/2	0	0.005917	yes
				1		no
19.963	$\nu\nu$	$1g$ 9/2	$1p$ 1/2	4		no
				5	0.014057	yes
20.006	$\pi\pi$	$3p$ 3/2	$1g$ 9/2	3	0.036733	yes
				4		no
				5	0.007479	yes
				6		no
20.034	$\nu\nu$	$3s$ 1/2	$2s$ 1/2	0	0.025183	yes
				1		no
20.206	$\nu\nu$	$3p$ 1/2	$1f$ 5/2	2	0.025746	yes
				3		no
20.473	$\pi\pi$	$1g$ 9/2	$1p$ 1/2	4		no
				5	0.012681	yes
20.495	$\pi\pi$	$2p$ 1/2	$1p$ 1/2	0	0.021261	yes
				5		no

With these parameters, a set of both proton and neutron single-particle states can be created. The Fermi energy is determined by filling the first Z proton levels and the first N neutron levels so that for both nucleon types the labels hole and particle can be assigned to the single-particle levels. We then obtain particle-hole quantum numbers for four types of nucleon-nucleon combinations using a combinatorial method. In our DWBA calculations, we include only the particle-hole pairs that obey parity and angular momentum conservation

$$(-1)^{l_h + l_p} = (-1)^J, \quad |j_h - j_p| \leq J \leq j_h + j_p, \tag{3.2}$$

where l_h, l_p are the orbital angular momentum and j_h, j_p the total angular momentum of the hole and particle, respectively. Equation (3.2) shows that we assume that J is equal to the transferred orbital angular momentum and this parity restriction excludes spin-transfer reactions from our analysis. Consequently, only normal-parity states are included. Equation (3.2) is consistent with our choice to consider a nucleon-nucleon interaction that consists of only a real, central term (see Sec. III B). Hence, inclusion of spin-transfer reactions in the present analysis would be inappropriate without the full

expression for $\mathcal{V}$, since a spin-independent ($S=0$) interaction will not excite non-normal parity states [24]. As an example, Table I shows part of the proton-particle neutron-hole level scheme, around 20 MeV of excitation energy for ^{90}Zr, that we include in our DWBA calculations.

B. DWBA calculations

Our calculations are performed with a target assumed to be in a 0^+ ground state. Reference [25] presents an extension of the one-component MSD formalism for nonzero target spins, by supplying the one-step direct cross section with the angular momentum factors that appear in conventional direct reaction theory. Since this extension has a sizeable impact only on the residual spin distribution, which we do not consider in this paper, we always start from a 0^+ ground state to keep our calculations tractable.

All DWBA matrix elements are calculated with the nuclear reaction code ECIS95 [26]. The scattering states are computed using an optical model potential, which we discuss later when we look at some specific reactions. We only consider the real, central term of the effective nucleon-nucleon interaction $\mathcal{V}_{ij}$, for which we take a Yukawa potential

$$\mathcal{V}_{ij}=-V_{ij}\frac{r}{r_0}\exp\left(-\frac{r}{r_0}\right), \tag{3.3}$$

with range $r_0=1$ fm and strength V_{ij}. This strength is taken as the only adjustable parameter in our MSD calculations. Although we use a shell model based on a harmonic oscillator to locate the single-particle states (mainly for its convenient analytical properties), it is physically more justified to determine the bound state wave functions with a Woods-Saxon potential. Its parameters are a reduced radius of 1.2 fm and a diffuseness of 0.6 fm. We take a starting value of 50 MeV for the potential depth and let ECIS95 search for the true value. We do not include a nonlocality correction (this may slightly affect the normalization [13]).

For a DWBA calculation with ECIS95, the excitation energy (and not the separate particle and hole energies) needs to be specified. In the present work, we assume that the excited particle is always bound, even if the finite depth of the hole forbids this, due to restrictions in currently available DWBA codes. The bound/unbound character of the excited particle is an aspect that may have a significant impact in more realistic MSD calculations. Clearly, the DWBA processes can involve unbound particle excitations. If $E_x>E_B$ (binding energy), there is a nonzero probability that the excited particle is in the continuum. If $E_x\geq E_F+E_B$, all particle states are unbound. Inclusion of DWBA matrix elements for unbound states may turn out to be an essential ingredient for an MSD analysis, but although progress in this direction has been made [27], we feel that the theoretical uncertainty in such calculations is still too large to justify inclusion in the present work.

IV. COMPUTATION OF THE MULTISTEP DIRECT EQUATIONS

The shell model of Sec. III A and the DWBA reaction mechanism as described in Sec. III B enable us to compute the MSD equations of Sec. II. The neutron and proton cross terms of the two-component MSD model imply that in general all possible combinations of particle-hole states can appear in a multistep process. Usually, we are interested in the simultaneous calculation of, e.g., (p,xn) and (p,xp) spectra and this requires one-step (p,n) reactions (exciting π particles and ν holes), (n,n') and (p,p') reactions (exciting both π particles, π holes and ν particles, ν holes), and one-step (n,p) reactions (exciting ν particles and π holes).

For both the fully microscopic or the state density approach, we preferably calculate DWBA cross sections for *all* particle-hole states that are prescribed by the shell model. Obviously, for the fully microscopic approach this is a necessity, and for the state-density approach this avoids any statistical uncertainty related to sampling of particle-hole states. In addition, we consistently include all particle-hole states for the lower incident energies that are required in the calculation of one-step cross section for the final step of the multistep expression (2.12). It is clear that the MSD calculations can get quite involved: a typical computation of 80 MeV (p,xn) and (p,xp) spectra on ^{90}Zr requires more than 60 000 individual DWBA cross section calculations.

The calculation of Eqs. (2.2) and (2.8) requires an expression for $\hat{\rho}_\mu$. Following Tamura *et al.* [4], we assume that a particle-hole state is distributed over the real nuclear states by a Gaussian distribution,

$$\hat{\rho}_\mu(p_\pi,h_\pi,p_\nu,h_\nu,E_x)\equiv G(E_\mu,E_x) = \frac{1}{\Gamma\sqrt{2\pi}}\exp\left(-\frac{(E_\mu-E_x)^2}{2\Gamma^2}\right), \tag{4.1}$$

where E_μ is the energy of the $1p1h$ state, determined by using Eq. (3.1) for both the particle and the hole, and Γ is the spreading width which we take equal to 4 MeV (corresponding to a full-width at half-maximum of 9.4 MeV). Note that we adopt the same expression for all four types of particle-hole pairs. The width Γ can be regarded as a measure of the effects of the residual interaction within the nucleus. It can also be viewed as a phenomenological way to account for other limitations and uncertainties in our approach. For instance, it can be thought of accounting for the effects of the splitting of the single-particle states due to deformation, and uncertainties in the exact location of the single-particle energies. Finally, continuum emission spectra tend to be structureless, and Eq. (4.1) ensures our theoretical results do not show significant structure.

All the tools to obtain double-differential spectra are now available. We sort all particle-hole states in classes of J, which gives the one-step cross section for transitions to states with spin J as

$$\frac{d^2\sigma_{j\leftarrow i}^{(1)J}(E,\Omega\leftarrow E_0,\Omega_0)}{d\Omega dE} = \frac{m^2}{(2\pi\hbar^2)^2}\frac{k}{k_0}\frac{1}{S}\sum_{\mu\{J\}}G(E_\mu,E_x)|\langle\chi_j^{(-)}(E,\Omega)| \times\langle\mu(p_\pi,h_\pi,p_\nu,h_\nu)|\mathcal{V}|0\rangle|\chi_i^{(+)}(E_0,\Omega_0)\rangle|^2, \tag{4.2}$$

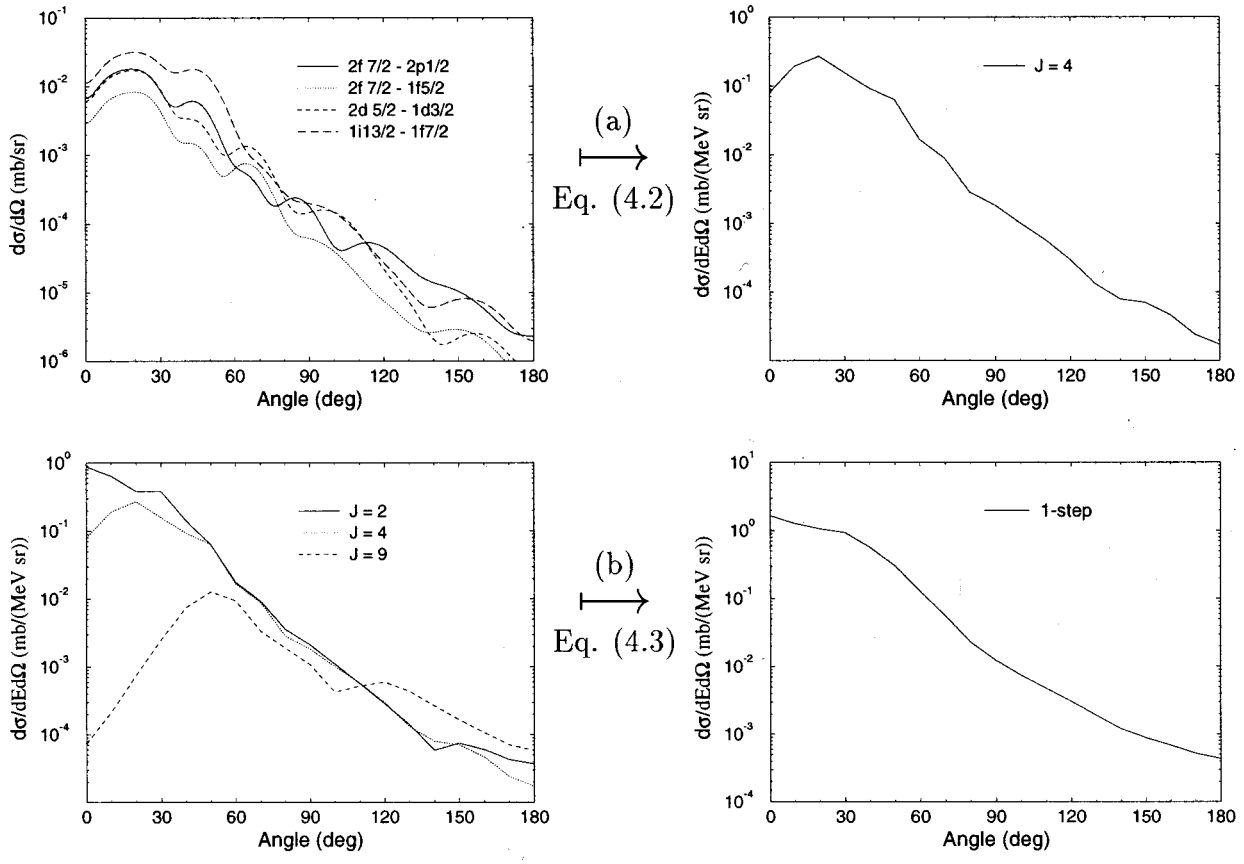

FIG. 3. (a) Gaussian average of DWBA cross sections for particle-hole states with $J=4$ around an excitation energy of 20 MeV, for a 80 MeV (p,p') reaction on ^{90}Zr. Only four particle holes are drawn. The result is a continuum double-differential one-step cross section for $J=4$. (b) Construction of the total one-step cross section from the several J components. Only three J-dependent cross sections are plotted. Each J component is multiplied by $2J+1$ according to Eq. (4.3).

where the sum $\Sigma_{\mu\{J\}}$ runs over all particle-hole states restricted to the J under consideration. A $1p1h$ state is only accounted for once in Eq. (4.2), i.e., a $(2J+1)$-fold degeneracy is not included. In numerical applications, the actual calculation of this cross section requires a renormalization, which is represented by S. The definition of S can be explained as follows. The complete one-step spectrum is *not* simply obtained by calculating DWBA cross sections for all shell model states at their exact energies E_μ, and subsequently spreading these DWBA cross sections with $G(E_\mu,E_x)$.[2] Instead, the shell model *states*, and *not* their cross sections, are distributed over the real states. The cross sections are determined for an excitation energy E_x (or, equivalent, an outgoing energy E) and accordingly for each E_x on the one-step energy grid the whole sum over μ applies. Hence, in principle we must calculate DWBA cross sections at the considered E_x, with the associated optical potential, for all particle-hole states. In practice, we only include particle-hole states that are within $\pm 2\Gamma$ of E_x. This cutoff of the Gaussian accounts, in an average way, for 95.44% (i.e., $S=0.9544$) of the total contribution and is a very reliable approximation. By dividing by S in Eq. (4.2), we ensure an exact normalization over the whole outgoing spectrum. In Fig. 3(a), four individual DWBA cross sections are plotted that take part in the construction of Eq. (4.2). In reality, several tens to a few hundred DWBA cross sections per J are included in our calculations. Note that the resulting angular distribution is already fairly structureless.

The continuum one-step cross sections (4.2) are calculated on an equidistant grid of outgoing energies. For the first step, we perform calculations at every 1 MeV of outgoing energy so that any remaining structural details are included. The one-step cross sections that are needed for the multistep terms are calculated on a grid of twelve equidistant energies (including the incident energy and the lowest energy grid point), which is followed by interpolation. The strength V_{ij} has an exponential dependence on the incident energy, see Sec. VII B, which is taken into account throughout the whole multistep calculation, i.e., at the lower intermediate energies, a higher value for V_{ij} is used.

Equation (4.2) is the starting point for both the fully microscopic MSD model and the model involving state densities.

A. Fully microscopic model

A calculation of DWBA cross sections for all $1p1h$ states ensures that no further approximations for the number of accessible states, and their spin distribution, in the con-

[2]We have investigated this other method, which is computationally far simpler. However, it is physically harder to justify, since the exact outgoing energies are not used in the DWBA calculations.

tinuum are required. The physical assumption is that the Gaussian broadened Nilsson model provides an adequate structure description of the continuum. The one-step cross section can then immediately be calculated. Since each particle-hole state is $(2J+1)$-fold degenerate, it is given by

$$\frac{d^2\sigma^{(1)}_{j\leftarrow i}(E,\Omega\leftarrow E_0,\Omega_0)}{d\Omega dE}=\sum_J\ (2J+1)\times\frac{d^2\sigma^{(1)J}_{j\leftarrow i}(E,\Omega\leftarrow E_0,\Omega_0)}{d\Omega dE}. \quad (4.3)$$

The process is depicted in Fig. 3(b). Again, the higher steps are obtained with Eqs. (2.9)–(2.12) by consistently using Eq. (4.3) for lower incident (i.e., intermediate) energies.

We mention here that our calculational approach is involved, but tractable because each shell model state is included only once in Eq. (4.2), assuming the state is completely degenerate. The more realistic splitting is then taken into account phenomenologically in an approximate way, by the Gaussian distribution (4.1), after the DWBA calculation. Table I provides another explanation of the construction of Eqs. (4.2)–(4.3).

We do not specifically include more sophisticated treatments of the particle-hole excitations, such as the influence of pairing effects, etc. Such refinements can be included in future work.

B. State densities

The exact MSD calculation as given by Eq. (4.3) along with the corresponding multistep terms is physically attractive because it consistently uses the shell model for both the DWBA and the nuclear structure part of the calculation. With such an approach, additional uncertainties concerning state density parametrizations are avoided. Nevertheless, it is still useful to make the connection with the approach that uses state densities. Then, we do not use the shell model to estimate the total number of states but only employ it as a tool to construct the averaged DWBA cross section. Instead of including the $(2J+1)$ degeneracy of each state, the computation is now performed with Eqs. (2.14)–(2.16). Since we have already determined the exact J-dependent cross section (4.2), it is straightforward to obtain the required averaged DWBA cross section. It is given by

$$\left\langle\frac{d\sigma_{j\leftarrow i}(E,\Omega\leftarrow E_0,\Omega_0)}{d\Omega}\right\rangle^{\mathcal{V}}_J = P\frac{d^2\sigma^{(1)J}_{j\leftarrow i}(E,\Omega\leftarrow E_0,\Omega_0)}{d\Omega dE}\Big/\,S_J(E_x), \quad (4.4)$$

where $S_J(E_x)$ is the sum of all Gaussian contributions from the $1p1h$ states to the outgoing energy E:

$$S_J(E_x)=\sum_{\mu\{J\}=E_x-2\Gamma}^{E_x+2\Gamma} G(E_\mu,E_x). \quad (4.5)$$

An important point to note is that we included a parity-conserving factor P in the average (4.4). The reason is that the state density (2.18) accounts for *all* particle-hole states, including those that can only be excited by spin-transfer reactions. However, in Sec. III A we noted that the averaged DWBA cross sections are constructed from non-spin-transfer reactions only. They are thus uncorrectly enhanced and this overestimation may be close to a factor of 2 (in the case of vanishingly small contributions from spin-transfer reactions), since non-natural parity states constitute 50% of all the states in a completely statistical model. We take $P=\frac{1}{2}$ which implies that we assume that spin-transfer contributions are zero. Clearly, calculations with more sophisticated interactions are required, but in the present calculation scheme P, which can easily be changed if required, serves as a patch-up for not including spin-dependent interactions and non-normal parity states. The P factor appears explicitly only in the state density approach. In fully microscopic calculations, the omission of non-natural parity states is effectively reflected by an extracted value of V_{ij} that is somewhat higher than the value of an approach that would include all noncentral terms (the strength would be divided over several components).

V. COMPARISON WITH CONVENTIONAL MSD METHODS

The method described in this paper features several new approaches towards calculating the MSD equations. The most conspicuous are the extension to a two-component formalism and the completely microscopic description including a spreading of the particle-hole states with Gaussian distributions. We will now compare several aspects of our method with conventional approaches that have been used in the past.

A. One component versus two component

The implications of using a two-component formalism instead of a one-component formalism have been discussed for semiclassical preequilibrium models in Refs. [28–30]. In an MSD context, the discussion falls into two aspects: state densities and DWBA matrix elements. The basic state density issue is that in a one-component model *all* nucleon-nucleon combinations of excited $1p1h$ states are included. This is unphysical, since charge conservation forbids the creation of certain particle-hole pairs in a one-step reaction. The main issue regarding DWBA matrix elements is that they should be computed with the appropriate types of excited particles and with the correct type of incoming and outgoing particle. The latter aspect has been taken into account for the one-step cross section but never for the multistep case.

The one-component version of the one-step direct cross section (2.14) is

$$\frac{d^2\sigma^{(1)}_{j\leftarrow i}(E,\Omega\leftarrow E_0,\Omega_0)}{d\Omega dE}=\sum_J\ (2J+1)R_n(J)\omega(1,1,E_x)\times\left\langle\frac{d\sigma_{j\leftarrow i}(E,\Omega\leftarrow E_0,\Omega_0)}{d\Omega}\right\rangle^{\mathcal{V}}_J, \quad (5.1)$$

where

$$\omega(p,h,E_x)=\frac{g^{p+h}}{p!h!(n-1)!}\sum_{k=0}^{h}(-1)^k\binom{h}{k}\times(E_x-\Delta-A_{\rm Pauli}-kE_F)^{n-1}\times\Theta(E_x-\Delta-E_{PP}-kE_F),\qquad(5.2)$$

where $g=A/13$, $A_{\rm Pauli}=[p^2+h^2+p-3h]/4g$, and $E_{PP}=[p2+h^2+p-h]/2g$. In the one-component model, this state density has been used for both inelastic scattering and charge exchange reactions. Hence, in the whole calculation, there is only a distinction between neutrons and protons in the description of the initial and final scattering state of the DWBA matrix element. Comparison with Eqs. (2.15) and (2.16) shows that the accessible $1p1h$ state density, calculated with Eq. (5.2) for a one-step (p,n) or (n,p) reaction is approximately (for $Z\approx N$) four times larger compared to that found in a two-component approach, and for inelastic scattering it is about twice as large. This is important, since once the state density (and optical model) parameters are fixed, the strength of the effective interaction $\mathcal{V}$ is the only remaining parameter that determines the magnitude of the computed cross section. This strength is usually labeled $V_0=\frac{1}{2}[V_{\pi\pi(\nu\nu)}+V_{\pi\nu}]$ in a one-component approach. Clearly, the reduced number of accessible states directly affects the absolute value of V_0 [31,32]. For incident energies where only the one-step direct cross section is significant (below about 30 MeV), it is possible to perform a one-component analysis and to estimate correction factors [13] for V_0 that approximates the effects of a neutron/proton distinction.

Applying correction factors on V_0 becomes more cumbersome for the multistep terms. In Sec. II B we have seen that numerous cross terms between nucleon types of both excited $1p1h$ states *and* leading particles occur. We argue that there is no longer a reasonable approximation possible that connects the one-component approach with the two-component approach. The only assumption that would enable such a connection is that the DWBA matrix elements are not only independent of the nucleon type of the $1p1h$ pair, which is a reasonable approximation for a simple Yukawa interaction, but also independent of the type of incoming and outgoing nucleon. The latter approximation is questionable: a one-step (p,n) cross section is different from a (p,p') cross section —it is imperative to treat the incoming and outgoing channel with the proper nucleon properties and their respective adequate optical potentials. However, in one-component implementations of the FKK model this approximation is necessarily implicit for the multistep terms. We will explain the difference with our two-component approach for both inelastic scattering and charge exchange. First, we take the simple case $V_{\pi\nu}=V_{\pi\pi}$. For the two-step direct contribution to a (p,p') process, we include the $(p,n)(n,p')$ term in addition to the $(p,p'')(p'',p')$ term. In terms of state densities, the statistical weight of the former reaction path is

$$g_\pi^2 g_\nu^2\propto Z^2N^2\quad\left(=\frac{A^4}{16}\quad\text{for } Z=N\right),\qquad(5.3)$$

and that of the latter

$$(g_\pi^2+g_\nu^2)(g_\pi^2+g_\nu^2)\propto Z^4+N^4+2Z^2N^2\quad\left(=\frac{A^4}{4}\quad\text{for } Z=N\right),\qquad(5.4)$$

whereas in a one-component approach one has a statistical weight of

$$g^4\propto A^4.\qquad(5.5)$$

In the one-component model, the contribution from $(p,n)(n,p)$ reactions is automatically included in Eq. (5.5), although the associated DWBA matrix elements are not calculated [only the (p,p') DWBA cross sections are used in one-component models]. Also, we conclude that for two-step inelastic scattering only 5/16 (for $Z=N$) of all accessible $2p2h$ configurations are involved. In general, the correction factor C_n for a n-step direct reaction with $Z=N$ is

$$C_n=\frac{S_n}{2^{2n}},\qquad(5.6)$$

where S_n is given by Eq. (2.13). Applying this correction factor to a one-component model directly affects V_0. Since the $(p,p'')(p'',p')$ term has a weight that is four times larger, the consequences of not explicitly calculating the $(p,n)(n,p)$ route may not be too drastic for a two-step process.

For (p,n) reactions, the one-component problem is more severe. The two-step cross section consists of a $(p,n')(n',n)$ and a $(p,p')(p',n)$ term. This time the statistical weights of the two routes are the same (both $A^4/8$, and again A^4 for the one-component case). Again, the problem is that a one-component state density does not provide a natural division between the $(p,n')(n',n)$ and $(p,p')(p',n)$ routes, whereas this division is automatically present in a two-component approach. So far, MSD calculations of (p,n) reactions have either assumed that the charge exchange part of the reaction takes place in the first step (in Ref. [33]) or have employed unphysical $(p,n)(p,n)$ convolutions (all other works), i.e., by assuming an independence on the nucleon type of leading particle and repeatingly taking the charge exchange matrix element as basis for a multistep calculation.

Using Eq. (5.6) we see that differences in the accessible phase space result in the correction factor for (p,p') reactions being twice that for (p,n) reactions in the first step. However, as the number of multistep scatterings increases, the ratio of these correction factors tends to unity, since the sensitivity to the initial channel projectile-type decreases with increasing scatterings.

The correction factors can be generalized to the case of $N\neq Z$ and $V_{\pi\pi}(=V_{\nu\nu})\neq V_{\pi\nu}$. The DWBA cross sections are proportional to V_{ij}^2. Therefore, we write the one-step direct cross section as

$$\frac{d^2\sigma_{j\leftarrow i}^{(1)}(E,\Omega\leftarrow E_0,\Omega_0)}{d\Omega\,dE}=\sigma_1\langle\text{m.e.}\rangle,\qquad(5.7)$$

where $\langle\text{m.e.}\rangle$ is a factor that includes the matrix element. Again, to relate to the one-component approach we must

assume that these matrix elements are the same for p-n or p-p interactions when applied in multistep calculations. For the one-component model,

$$\sigma_1 = V_0^2 g^2, \tag{5.8}$$

for both (p,n) and (p,p') reactions. In the two-component model, σ_1 should be replaced by

$$\sigma_1^{\pi\pi} = V_{\pi\pi}^2 g_\pi^2 + V_{\pi\nu}^2 g_\nu^2, \tag{5.9}$$

for (p,p') reactions, and

$$\sigma_1^{\pi\nu} = V_{\pi\nu}^2 g_\pi g_\nu, \tag{5.10}$$

for (p,n) reactions. The correction factors can be written down as recursive relations due to the convolution structure of the FKK theory. For (p,p') we have

$$C_n = \frac{\sigma_n^{\pi\pi}}{\sigma_n}, \tag{5.11}$$

and for (p,n) reactions we have

$$C_n = \frac{\sigma_n^{\pi\nu}}{\sigma_n}, \tag{5.12}$$

where

$$\begin{aligned} \sigma_n^{\pi\pi} &= \sigma_{n-1}^{\pi\pi}\sigma_1^{\pi\pi} + \sigma_{n-1}^{\pi\nu}\sigma_1^{\nu\pi}, \\ \sigma_n^{\pi\nu} &= \sigma_{n-1}^{\pi\pi}\sigma_1^{\pi\nu} + \sigma_{n-1}^{\pi\nu}\sigma_1^{\nu\nu}, \\ \sigma_n &= \sigma_{n-1}\sigma_1 . \end{aligned} \tag{5.13}$$

In the limit of $Z=N$ and $V_{\pi\pi}=V_{\pi\nu}$, these correction factors reduce to Eq. (5.6).

In sum, we believe that an MSD analysis should include a distinction between neutrons and protons at all levels of the calculation: (1) a two-component state density or, better, a fully microscopical analysis, (2) a two-component effective interaction, (3) the appropriate nucleon type of particle and hole in the DWBA matrix element, and (4) the correct type of leading particle at the initial, intermediate and final stage of the MSD reaction. These are all accounted for by the equations of Sec. II. Correction factors are not needed, though we have provided them for completeness.

B. Sampling

The conventional method [32,34] for obtaining an averaged DWBA cross section is to select several (typically about eight) particle-hole states with the same J that are located within a certain width around a considered excitation energy E_x. Then, for each (E_x,J) class, the corresponding individual DWBA cross sections are calculated, summed, and divided by the number of states included. For certain J, the aforementioned number of states may be found within, say, ± 4 MeV around E_x, which ensures a reasonable statistical average. For other J, however, the lack of nearby states leads to the inclusion of states that are very far from the energy of interest. In addition, the simple arithmetic average means that each state in the sample is treated as equally important, regardless of its position relative to E_x. This can lead to an unphysical representation of the real nuclear state at the considered energy. Our approach with a Gaussian spreading of the $1p1h$ states appropriately emphasizes the model states that are close to the outgoing channel energy.

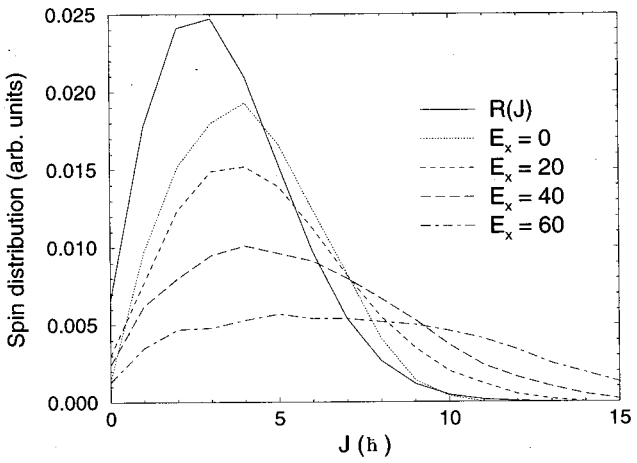

FIG. 4. Spin distribution of Nilsson model states around various excitation energies. The solid curve represents the Wigner-type spin distribution (2.19).

We appreciate that a physically inconsistent aspect of our state density approach as well as the older one-component approaches is that the averaged DWBA cross section is based on shell model states whereas it is multiplied by a state density that is based on equidistant single-particle levels. Ideally, a quantum-mechanical preequilibrium analysis should be performed either completely microscopically, or with more realistic state densities (e.g., by using microscopic single-particle levels).

An important factor for the averaged DWBA cross section is the normal-parity states issue, which has not been taken into account in previous analyses. The factor P of Eq. (4.4) clearly has an impact on the strength of the effective interaction that is extracted in an analysis of data.

C. Spin distribution

Our fully microscopic approach has revealed another problem that is already known but has not yet been discussed within an MSD context. With increasing excitation energies, the abundance of $1p1h$ states with high spin increases. This phenomenon is not reflected by the spin distribution (2.19) which is independent of energy. Figure 4 displays the J distribution of the $1p1h$ states for several excitation energies as predicted by the spherical Nilsson model, compared with the spin distribution (2.19). Not only is the J distribution broader at high excitation energies, also its Wigner-type shape disappears (which is not surprising since the underlying assumption is based on statistical arguments, and when the number of degrees of freedom is just 2, such arguments cannot be expected to hold well). A partial solution to this problem is to adopt an energy dependent spin cutoff factor for MSD methods involving state densities. This results in a J distribution that has an increasing width for increasing excitation energies. A formula was proposed by Herman and Reffo

TABLE II. Values of the strength of the effective interaction for the reactions studied in this paper.

Nuclide	Reaction	Energy	$V_{\pi,\nu}$	$V_{\pi,\pi}$	$V_{\nu,\nu}$
^{90}Zr	(n,xn)	14			23.9
^{90}Zr	(n,xn)	18			23.3
^{90}Zr	(p,xn)	25	26.2		
^{90}Zr	(p,xn)	45	25.3		
^{90}Zr	(p,xn)	80	17.3	17.3	17.3
^{27}Al	(p,xp)	90	20.1	20.1	20.1
^{27}Al	(p,xn)	90	20.1	20.1	20.1
^{27}Al	(p,xn)	113	16.9	16.9	16.9
^{56}Fe	(p,xn)	113	13.1	13.1	13.1
^{208}Pb	(n,xn)	14			22.3
^{208}Pb	(p,xn)	113	14.8	14.8	14.8

[35], who studied shell model particle-hole configurations up to 30 MeV of excitation energy:

$$\sigma^2(E_x)=(0.24+0.0038E_x)nA^{2/3}, \tag{5.14}$$

giving a wider spin distribution for increasing E_x. This formula certainly seems more realistic than Eq. (2.21) when compared with the shell model distribution, although it does not account for the aforementioned non-Wigner behavior. In Sec. VII, we show the impact of these assumptions on continuum angular distributions.

D. Implications for the strength of the effective interaction

The value of the strength of the effective interaction V_0 has been frequently discussed in MSD papers, see, e.g., Refs. [1,31,36]. Austin [37] performed an extensive analysis of inelastic scattering and charge exchange reactions to discrete states for incident energies below 50 MeV and has reported values of $V_{\pi\pi}=V_{\nu\nu}=12.7$ MeV, $V_{\pi\nu}=43.1$ MeV (and hence $V_0=27.9$ MeV) for the central Yukawa terms of $\mathcal{V}$. With this information coming from a completely independent source, MSD analyses were usually considered a success when these values could be reproduced from fitting continuum spectra. We feel that it is dangerous, however, to draw premature conclusions concerning reproducing Austin's values in an MSD analysis. Even when the same DWBA reaction parameters as those of Austin are used (see Sec. III B), there are remaining uncertainties such as the optical model employed [31], the omission of non-natural parity states (the effect of which is hided in the value of V_0), isospin conservation questions which have not yet been addressed, and a too simple prescription of the partial level density or, more generally, the single-particle level scheme. These aspects were not discussed in Ref. [37], but have a significant impact on the results.

As mentioned previously, a discussion of correction factors to distinguish between protons and neutrons within one-component models was given in Refs. [13,31,32]. In Table II the values of $V_{\pi\pi}$, $V_{\nu\nu}$, and $V_{\pi\nu}$ that we extracted from fitting various sets of double-differential and angle-integrated spectra are displayed. We will now relate our two-component results to the values of V_0 obtained from previous FKK analyses. This can be done by considering cases where the one-step component is dominant. First, the natural parity-states factor P has never been included in the DWBA average and inclusion of our approximation $P=1/2$ would reduce the one-step direct cross section by a factor of 2. Then, for charge exchange reactions the state density is about four times smaller in a two-component approach and about twice as small for inelastic scattering. Hence, if we would apply these natural-parity and state density arguments as corrections on previous results (using DWBA matrix elements independent of nucleon type) we conclude that the values for V_0 as reported in previous works should actually be $\sqrt{8}$ times larger for charge exchange and twice as large for inelastic scattering. This leads to unacceptable high values if applied on the older results for V_0, some of which are quite close to Austin's values. A possible explanation for this may be provided by the application of the DWBA method [38]. The correction factors (5.6) for the higher steps have an additional slight effect on the extracted value of V_0.

E. Isospin considerations

Conservation of isospin in preequilibrium reactions is not included in the present work; rather, we consider the theoretical formalism and practical implementation of isospin considerations to be an important area for future study within quantum-mechanical preequilibrium theory. However, here we address the likely impact of isospin considerations on the predicted cross sections for the reactions under study in this work. Our considerations are based mainly upon such studies in the context of the semiclassical exciton preequilibrium model. We note, however, that one of the advances presented in this work, namely, the distinction between neutron and proton particle-hole excitations within the preequilibrium cascade, is an essential (albeit preliminary) step in such considerations.

Kalbach has developed an exciton model that allows the study of the role of isospin conservation or mixing in the preequilibrium phase of a reaction [39–41]. Either completely mixed, or completely unmixed (conserved), isospin can be assumed in the calculations. (Our work corresponds to an assumption of complete isospin mixing.) Grimes' recent studies [42] on the role of isospin conservation in neutron-induced compound nucleus reactions demonstrated that in certain reactions (particularly for light nuclei), α emission can be significantly enhanced, though the impact on proton and deuteron decay is minor. In Refs. [43,44] Watanabe has discussed the possible implications of isospin within the exciton and multistep compound FKK theories. These studies typically assume that isospin is conserved in the preequilibrium stage of the reaction, and about 50% isospin mixing occurs at equilibrium. However, as discussed below, in some cases preequilibrium neutron and proton spectra are insensitive to isospin considerations.

Watanabe *et al.* noted [44] that isospin considerations have most influence in (p,xp) reactions at low incident energies, near the (p,n) threshold energy [e.g., below 14 MeV for (p,p') reactions on nuclei near $A=100$], but the impact of isospin conservation decreases at higher energies for these reactions. In proton-induced reactions, both $T^<=T_0-1/2$ and $T^>=T_0+1/2$ states, T_0 being the z component of the target isospin, can be excited in the composite nucleus,

whereas in neutron-induced reactions only one isospin state in the composite nucleus can be excited, $T^{>}=T_0+1/2$. In proton-induced reactions, if isospin mixing is assumed not to occur, particle decay from the two different isospin states $T^{<}$ and $T^{>}$ should be considered. Isospin conservation is particularly important, resulting in an enhanced proton emission, if neutron emission from $T^{>}$ states is suppressed by an isospin selection rule. But as the incident energy (and the composite nucleus excitation energy) increases, neutron decay from the $T^{>}$ composite nucleus states to $T^{>}$ states of the residual nucleus becomes open, and an increased fraction of the flux in the $T^{>}$ composite nucleus decays into this neutron, instead of proton, channel.

The results of Kalbach's exciton model calculations [41,45] with and without isospin conservation, for the preequilibrium reactions studied in this paper, are useful for assessing the likely impact of isospin within an FKK approach. Calculated differences in the magnitude of preequilibrium spectra for the two isospin assumptions (complete conservation, and complete mixing) are as follows: for Zr(n,xn) at 14 and 18 MeV, and Pb(n,xn) at 14 MeV–$<$2%; Zr(p,xn) at 25, and 45 MeV–$<$10%. The other (p,xn) and (p,xp) reactions at 80 and 113 MeV – approx $<$15–20 %.

Therefore, one of the conclusions of Kalbach's work is that in some cases preequilibrium spectra are not sensitive to the isospin conservation/mixing (in particular, the reactions we study below 45 MeV). In other cases, isospin conservation versus mixing plays a larger role, and influences the calculated results at a level a little smaller than the typical predictive capability of preequilibrium theory calculations (about 20–25 %). However, the experimental evidence supporting isospin conservation, or mixing, in preequilibrium reactions at higher energies is inconclusive. Although the short lifetimes of preequilibrium particle-hole stages would suggest that isospin conservation is a reasonable assumption in preequilibrium reactions, in some cases exciton model calculations that assume complete mixing appear to describe measured data most accurately [45]. Feinstein [46] has discussed the importance of isospin mixing in preequilibrium reactions within the context of the FKK theory, though applied to photonuclear reactions.

In conclusion, the role of isospin conservation in MSD reactions is an important area for future study. The reactions considered in this work below 45 MeV are probably rather insensitive to isospin considerations, though semiclassical studies suggest larger sensitivities for the higher-energy reactions. At present, shortcomings in the present approach (which, for simplicity, implicitly assumes complete isospin mixing) translate into inaccuracies in the extracted value of the (only) parameter in the theory: the residual interaction strength. Since the cross sections vary as the square of this parameter for the dominant one-step scattering, possible uncertainties in the residual interaction in the present approach may be up to 7–10 %.

VI. OTHER REACTION MODELS INCLUDED

A. Direct reactions to discrete states

Although our work is primarily directed towards reactions to the continuum, we aim at a full treatment of direct, discrete effects at low excitation energies. In this way we can avoid a simulation of the collective part of the spectrum by the incoherent continuum MSD mechanism. A method to include these collective effects is described in Refs. [33,47] and we follow that approach here with a slight modification. In order not to miss any collective strength, our calculations include all discrete levels of the nucleus for which the spin, parity, and deformation lengths δ_L are known. The deformation lengths are automatically transformed to deformation parameters for each different component of the optical potential. For each level, ECIS95 calculates the direct inelastic cross section with coupled channels, for the first few states or DWBA, for the higher lying states, with a nuclear structure model (vibrational, rotational, etc.) that is appropriate for the nucleus under study.

In order to compare the calculated cross sections for all states included with experimental double-differential spectra for inelastic scattering, we simulate the experimental resolution and the spreading of the spectroscopic strength by a Gaussian broadening of the cross section for each discrete state. For (n,n') reactions, the width is typically 0.5 MeV. For proton-induced reaction spectra at higher incident energies, we usually combine the collective strength in energy bins of 1 MeV.

In Refs. [33,47], double counting of collective and MSD contributions was prevented by simply subtracting the smoothed collective cross section from the MSD cross sections. If the discrete level scheme of a nucleus is well known in terms of level energy, spin, parity, and deformation length, collective state calculations can be extended up to several MeV of excitation energy, and the continuum one-step direct contribution, which is now of a more effective nature, enters only gradually around this energy. On the other hand, if the discrete level scheme of a nucleus is almost or completely unknown, the cross sections at the highest outgoing energies are necessarily simulated by the continuum MSD mechanism.

A different method was proposed in Refs. [48,49] where it appears that the MSD cross section contributes a continuum background to the cross section for *all* discrete levels. This is in contradiction with our view that the first several states of a typical nucleus usually constitute a complete level scheme for the first few MeV, not allowing for any other direct-reaction-like background. A valuable aspect of Refs. [48,49], that is not yet considered in our work, is the energy weighted sum rule that provides an estimate of the giant resonance contributions to the continuum.

At present, we think that the most realistic approach lies between those of Refs. [33,47] and [48,49] and this is what is included in the present work. Level density matching between low-lying discrete states and the continuum provides an indication of missing (experimentally undetectable) levels after a certain cutoff level, and we let the MSD contribution gradually enter above this level. In our view, contributions from individual states above this level may be termed collective states in the continuum and we regard them as incoherent additions to the continuum one-step direct spectrum. From the point of view of nuclear structure, a more elegant method to avoid double counting would be to use an effective $1p1h$ state density that includes a correction for the presence of collective levels.

A benefit of including an extensive discrete level scheme for direct calculations is that it enables a more reliable estimate of the remainder of the reaction cross section that is provided by the other reaction mechanisms. This has different implications at various energies. At low incident energies, this affects the compound nucleus formation cross section, defined as the total reaction cross section minus the integrated direct and preequilibrium cross section, which is an essential ingredient for a precise calculation of the compound contribution. At high incident energies, when the primary emission cross section consists solely of direct and MSD contributions, the inclusion of a collective contribution slightly affects (reduces) the effective interaction parameters of the MSD part, since the total integrated MSD and direct cross section, summed over outgoing particle types, may not exceed the total reaction cross section.

B. Multistep compound reactions

Multistep compound (MSC) reactions occur for incident energies up to a few tens of MeV. In the MSC reaction mechanism, the stepwise reaction proceeds through the bound configurations of the composite nucleus. As with compound reactions, it is imagined that the incident particle is captured by the target nucleus but that emission takes place before the attainment of statistical equilibrium. For MSC reactions, we employ the model of Feshbach, Kerman, and Koonin [8]. Our implementation of the FKK formalism essentially follows the method of Chadwick and Young [50]. All transmission coefficients that appear in the MSC formula are calculated with ECIS95, using the same optical model as used for the other reaction mechanisms. For the level density, the Oblozinsky formula [51] is used. We are able to calculate MSC emission up to five steps, but in practice it is sufficient to include only two stages and to consider the remainder as r-stage (equilibrium) contribution, which we calculate with Hauser-Feshbach theory.

An important phenomenon in MSC theory is gradual absorption. The pure MSD process is based on the assumption that as soon as the reaction proceeds through the unbound chain, the particle-hole configuration will remain unbound until particle emission takes place. One may, however, imagine that the leading particle loses a large fraction of its initial kinetic energy after one or more successive collisions in a multistep process. Then, instead of the process of fast emission, some of the particle flux may flow into the bound chain and give rise to (multistep) compound emission. A tractable method for this $P \rightarrow Q$ crossover effect within the FKK theory has been discussed by Chadwick and Young [50] and by Marcinkowski *et al.* [52]. In our work, we adopt the method of Marcinkowski *et al.* and introduce a gradual absorption of the flux into subsequent reaction steps on the basis of level density ratios. It is important to note that this $P \rightarrow Q$ transition model effectively *reduces* the MSC contribution since a significant part of the non-MSD emission flux does not enter the $2p1h$ MSC stage from the initial stage but enters the $3p2h$ MSC stage from the MSD chain. The predominance of the damping width over the emission width for the $3p2h$ MSC stage then implies that this flux almost completely propagates to the equilibration stage, contributing to compound emission rather than MSC emission.

C. Compound reactions

We describe primary compound emission by the continuum Hauser-Feshbach formula. and use the Weisskopf-Ewing model for compound reactions after the first stage. For the total level density $\omega(E_x)$ we take the composite formula as proposed by Gilbert and Cameron [53] and incorporate shell effects in our calculations by adopting the method of Ignatyuk [54] for the level density parameter a. The shell correction δW can be eliminated from Ignatyuk's formula by imposing the boundary condition that at the binding energy the energy-dependent level density parameter as must coincide with a value determined from a conventional, energy-independent analysis [33]. Also, Ignatyuk *et al.* observed that extrapolating their formula to too low excitation energies may be dubious, which motivated us to keep the level density parameter constant below the neutron binding energy B. Together, this leads to the following parametrization of the energy-dependent level density parameter:

$$a(E_x) = a_B, \quad \text{if } E_x \leqslant B$$
$$= \overline{a}\left(1 - \frac{f(E_x)B(1-a_B/\overline{a})}{f(B)E_x}\right), \quad \text{if } E_x > B, \tag{6.1}$$

where a_B is the level density parameter at the neutron binding energy. For this, we use the formula of Ref. [55]. In Eq. (6.1),

$$\frac{\overline{a}}{A} = \alpha + \beta A, \tag{6.2}$$

with $\alpha = 0.154$ MeV^{-1} and $\beta = -6.3 \times 10^{-5}$ MeV^{-1}. The function $f(E_x)$ is given by

$$f(E_x) = 1 - \exp(-\gamma E_x), \tag{6.3}$$

where $\gamma = 0.054$ MeV^{-1}.

We include competition by neutrons, protons, deuterons, tritons, ^{3}He, α particles, and γ rays. Emission from secondary and higher stages of all these particles is taken into account until all possible outgoing channels are closed.

D. Multiple MSD reactions

For incident energies below about 50 MeV, one can safely assume that after primary preequilibrium emission the excitation energy of the residual nucleus is relatively small and that further decay of the nucleus proceeds by a pure compound mechanism. At higher incident energies such an assumption will result in an underprediction of the outgoing spectrum above the evaporation peak. This deficit stems from the omission of multiple preequilibrium emission: it is conceivable that after the first reaction the residual excitation energy is so high that another fast particle can be emitted before equilibration of the nucleus.

Since MSD is the predominant preequilibrium reaction mechanism, certainly if one includes $P \rightarrow Q$ transitions, one can safely assume that multiple pre-equilibrium emission proceeds by MSD only (this has been confirmed in Ref. [56]). An exact multiple MSD model would be extremely involved, since the residual state after primary emission is characterized by an excitation energy, a particle-hole con-

figuration, a residual spin (directly coupled to the primary angular distribution), and parity and the corresponding primary cross section has to be connected to a secondary double-differential calculation for another unbound leading particle. Even theoretically, such a task maybe practically feasible only for secondary MSD emission following one-step primary MSD emission, when the quantum numbers of the residual nucleus can still be unambiguously assigned to the excited $1p1h$ state. For comparison of theory and experiment, it is more tractable to consider an angle-integrated multiple MSD model and to make reasonable assumptions concerning the secondary angular distribution separately. The first initiatives in that direction have been taken in Ref. [32]. There, a multiple MSD formula is proposed that is based on the equiprobability assumption for particle-hole configurations:

$$\frac{d\sigma_{mpe}^{(j)}}{dE}=\sum_{N}\sum_{i=\pi,\nu}\int_{E_x=E+E_B}^{E_x^{\max}}\frac{d\sigma^{(N,i)}}{dE_x}\times\left[\frac{1}{p}\,\frac{\omega(1p,0,E+E_B)\,\omega(p-1,h,E_x-E-E_B)}{\omega(p,h,E_x)}R_N^{ij}\right]\times G(E)\,\mathrm{d}E_x\,, \tag{6.4}$$

where N is the primary MSD stage, and i, j label the nucleon type of the primary emitted particle and the secondary emitted particle. Equation (6.4) can be said to consist of three factors. The first factor $d\sigma^{(N,i)}/dE_x$ is the angle-integrated primary MSD cross section for each step and represents the feeding of a residual excitation energy channel E_x following primary emission. The second factor, the quantity between brackets, estimates the probability that at E_x there is an excited particle in the continuum. Obviously, the chance of finding such a particle is highest for a $1p1h$ configuration. Hence, one-step primary MSD emission is the most important feeding channel for multiple MSD emission. The factor R_N^{ij} is the probability of finding a particle of type j in class N after primary emission of type i. A prescription for R_N^{ij} can be found in Ref. [57]. The third factor $G(E)$ is a penetrability factor that describes the further propagation of the continuum particle: emission or capture. In practical calculations, we use the s-wave transmission coefficient for this penetrability, though a Gamow factor can also easily be used [58].

The energy dependence of G simulates the intuitively expected processes at each energy. For high particle energies this is close to unity and the particle is probably emitted, and for low energies it is close to zero, implying that the particle is likely to be captured in the bound chain. Still, this assumption restricts the number of alternatives for the continuum particle to 2: either it is immediately emitted at its original energy (minus the binding energy) or it disappears in the compound chain. Other possibilities for further propagation of the continuum particle are thereby excluded. Perhaps an extension of Feshbach's projection operator formalism can provide a sound physical theory for multiple preequilibrium emission [59].

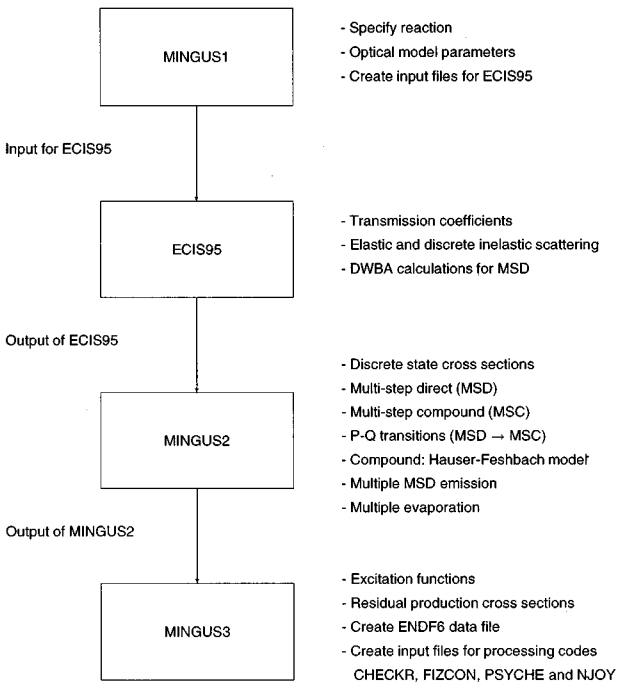

FIG. 5. Flow chart of the nuclear model code system MINGUS.

VII. RESULTS

A. The calculation scheme: MINGUS

By combining the direct, preequilibrium and compound nuclear models in one calculation we are able to predict double-differential spectra and residual production cross sections [60] for incident energies up to 200 MeV. The code system that performs this task, MINGUS, is schematically given in Fig. 5. It consists of four parts. The first part deals with the specification of the basic nuclear reaction information, such as optical model and nuclear structure parametrizations. With this information, it creates all necessary input files for the second part, ECIS95, which computes all basic transition amplitudes and cross sections that are required for the third part, MINGUS2, where the results as provided by ECIS95 are processed into double-differential spectra on the basis of the prescriptions given in this paper. The last part of the code system can be used to give excitation functions and to create an evaluated nuclear datafile (ENDF) for nuclear data applications (not discussed here). In MINGUS, the primary reaction cross section is composed as

$$\sigma_{\mathrm{reaction}}=\sigma_{\mathrm{direct}}+\sigma_{\mathrm{MSD}}+\sigma_{\mathrm{MSC}}+\sigma_{\mathrm{compound}}\,. \tag{7.1}$$

The direct, MSD, and MSC contributions are calculated first, after which the flux that goes in the compound channel is renormalized such that Eq. (7.1) automatically holds. When the first stage is completed, the calculation proceeds with secondary MSD emission and multiple compound emission. The latter processes are obviously not included in the sum rule (7.1).

B. Comparison with experimental data

Comparisons between preequilibrium models and experimental data have been performed in the energy region 10–

200 MeV. We distinguish three energy regimes, with different reaction mechanisms dominating the interpretation of measured cross sections in these regimes.

The first region covers incident energies up to 30 MeV. Of the MSD contribution, only the one-step component is important, so that any theoretical or numerical issues concerning higher steps are not probed here. On the other hand, there are simultaneous contributions of collective, MSD, MSC, and compound processes. This may give rise to some ambiguity: several reaction mechanisms can account for the observed cross section and more than one parameter (usually the level density parameter or V_{ij}) can be varied to fit the spectrum.

The second region covers energies between 30 and 60 MeV. Two- and three-step direct processes will give sizeable contributions to the spectrum, whereas the MSC contribution rapidly decreases for incident energies above 30 MeV. Capture in the Q chain that eventually leads to compound emission does, however, still account for a significant part of the reaction cross section.

Above 60 MeV, the situation for primary emission becomes relatively simple. Immediate capture in the MSC Q chain is very improbable and it can be assumed that the direct and MSD mechanisms completely cover the primary stage of the reaction. Accordingly, for these cases MINGUS performs a search on V_{ij}, by repeating the complete MSD calculation, until the integrated direct + MSD cross section is equal to the reaction cross section (independently determined by the optical model). Then, the only free parameter left is the $V_{\pi\pi}$ (or $V_{\nu\nu}$)/$V_{\pi\nu}$ ratio, while their sum is automatically determined. The additional complication that arises at these energies is that multiple preequilibrium emission now contributes to the inclusive emission spectra (though not at the very highest emission energies).

Figures 6 and 7 show a comparison between fully microscopical calculations and experimental data for 14 MeV double-differential (n,xn) spectra for ^{90}Zr and ^{208}Pb. In the figures, we have separated multiple compound emission [which includes processes such as $(n,2n)$, (n,pn), etc.] from primary compound emission. For the broadening of the discrete peaks, we used a width of 0.5 MeV. The results show that our approach of including direct cross sections for many discrete levels provides an adequate description of the fluctuations in the high-energy tail at all outgoing angles. Consequently, the effective continuum one-step direct contribution enters only after several MeV of excitation energy, as described in Sec. VI A. Globally, we obtain satisfactory agreement at all measured outgoing energies and angles for 14 MeV (n,xn) reactions. Exceptions are the prediction of the first discrete peak and the evaporation peak at 60° for ^{90}Zr. The optical models used for the various reactions, together with their references, can be found in Table III.

The 25 and 45 MeV (p,xn) reactions on ^{90}Zr, see Fig. 8, reveal the omission of the isobaric analog state peak in our calculations, since we do not include isospin considerations. However, the cross section for such excitations represent only a small fraction of the total neutron production. Also note that for the 45 MeV case multiple MSD emission is already present, though small, and that the MSC contribution has virtually disappeared.

We have chosen the 80 MeV double-differential (p,xp) reaction on ^{90}Zr to demonstrate the sensitivity to the optical model and level density parameters. The comparison of the fully microscopical approach with experimental data as displayed in Fig. 9(a) is obtained with Madland's optical model above 50 MeV and the Becchetti-Greenlees parametrization below 50 MeV. This results in a sizeable overestimation at the backward angles, even at an outgoing energy of 60 MeV. In Fig. 10 we show the same reaction but now predicted using Menet's potential above 20 MeV and Becchetti-Greenlees below 20 MeV. This optical model choice clearly improves the fit, although not yet to a satisfactory level. The calculated angular distribution changes significantly if we use the state density approach. Figure 9(b) shows the same reaction, again with the Madland and Becchetti-Greenlees potential and with the same set of DWBA matrix elements, but now with Eqs. (2.18)–(2.21) for the $1p1h$ state density. There is now excellent agreement with experiment. The reason is that in the fully microscopic approach, individual DWBA cross sections for several high-spin states give a rather flat contribution to the total sum, resulting in a less forward peaked angular distribution. When partial state densities are used, the Wigner-type spin distribution (2.20) strongly inhibits the contribution of these averaged DWBA cross sections for high J, leading to a good prediction in this specific case. The same reaction has been analyzed within one-component approaches Refs. [12,32,36], where also good agreement is found using Eq. (2.20). Figure 9(c) shows the effect of applying the energy dependent spin cutoff factor, Eq. (5.14). As expected, this leads to a flatter angular distribution. One should, at this stage, be cautious in drawing conclusions from this spin distribution phenomenon since at least two uncertainties remain. First, the examples show that the dependence on the use of the particular global optical model is rather sensitive. A dedicated proton optical potential for ^{90}Zr (of which we are unaware) should reduce this uncertainty. Second, a significant fraction of the particle-hole states around an excitation energy of 20 MeV are unbound —in our calculations they are assumed to be quasibound— and the influence of these transitions is still unknown. The angle-integrated (p,xn) and (p,xp) spectra are well predicted, see Figs. 10(a) and 10(b) and we note that the angle-integrated spectra are less sensitive to the optical model choice. Note that at an outgoing energy of 20 MeV there is a sizeable contribution from multiple MSD emission. For all reactions above 60 MeV, we assume $V_{\pi\nu}=V_{\pi\pi}=V_{\nu\nu}$. Next, MINGUS determines this value using the unitarity requirement.

Another case for which both (p,xn) and (p,xp) spectra exist is for the 90 MeV proton-induced reaction on ^{27}Al. In Fig. 11, calculations of double-differential and angle-integrated spectra are compared with measurements. For light nuclei, the density of shell model states is low, resulting in some fluctuations in the spectra when calculated with the fully microscopical approach. Note that the underprediction seen in Fig. 11(b) of our angle-integrated spectra compared to experimental data at the higher emission energies is partly an artifact of the angle-integration procedure used by Kalend *et al.* [70]. In Figure 12 of Ref. [70], Kalend *et al.* show how they extrapolate the angular distributions to small angles using a linear increase (when plotted on a logarithmic scale).

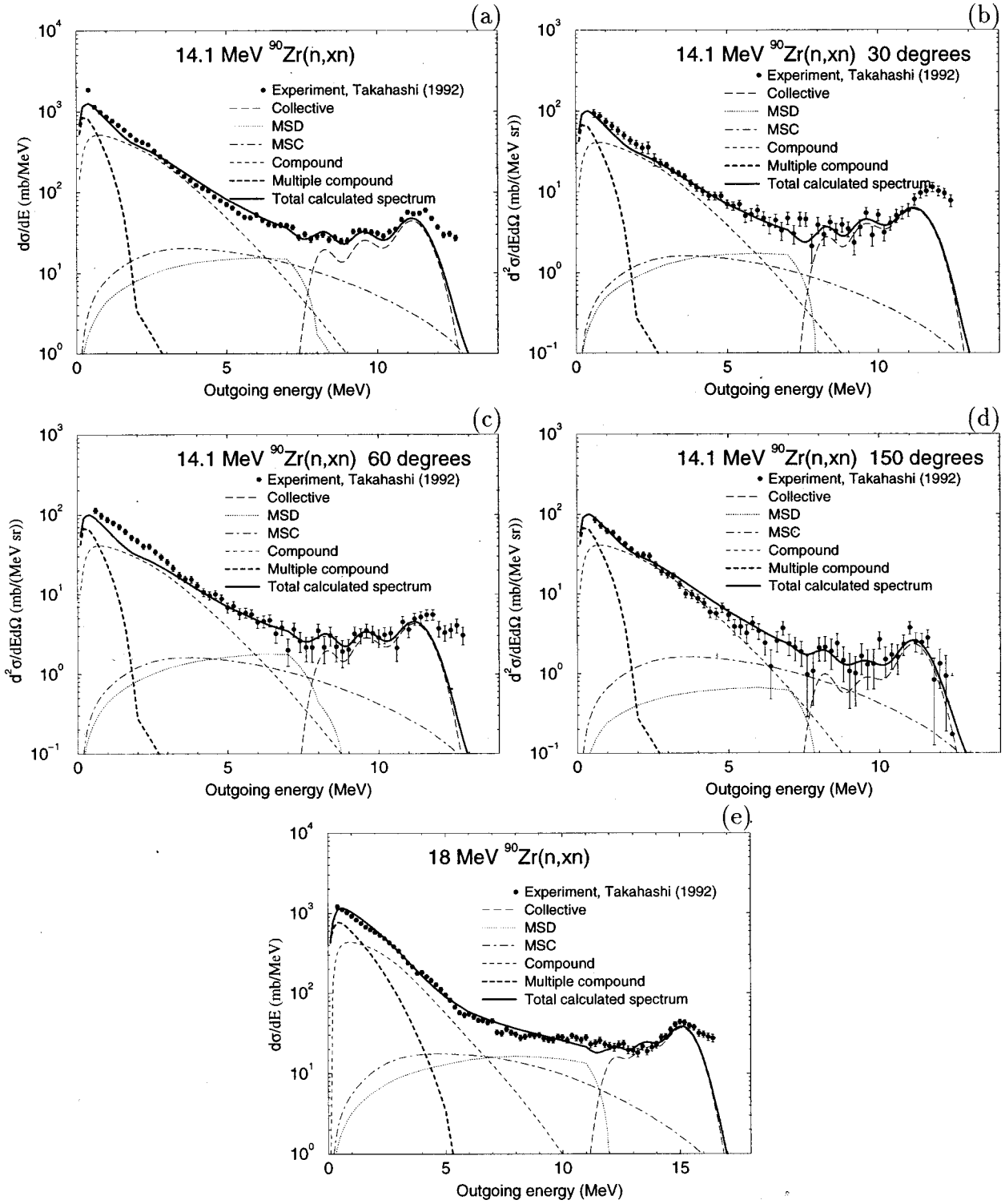

FIG. 6. Comparison of fully microscopical calculations with experimental data [66] for the ^{90}Zr(n,xn) reaction at 14.1 MeV: (a) angle-integrated spectrum, (b) 30°, (c) 60°, and (d) 150°, and (e) angle-integrated spectrum at 18 MeV.

However, both theoretical arguments [71] and systematics from measurements [9], indicate that a better functional form is a cosine shape, which becomes flat at small angles. Thus, for very forward-peaked angular distributions at the higher emission energies, Kalend's procedure can significantly overestimate the angle-integrated result. Better agreement with our calculations would be obtained in Fig. 11(b) if a more accurate angle-integration scheme was used to determine the experimental data.

At 113 MeV, double-differential (p,xn) spectra have been measured for several nuclides [72]. In Fig. 12, we show the comparison of MINGUS with the experimental data. When we compare this with the results from calculations with the high-energy transport code HETC [72], we see that the differ-

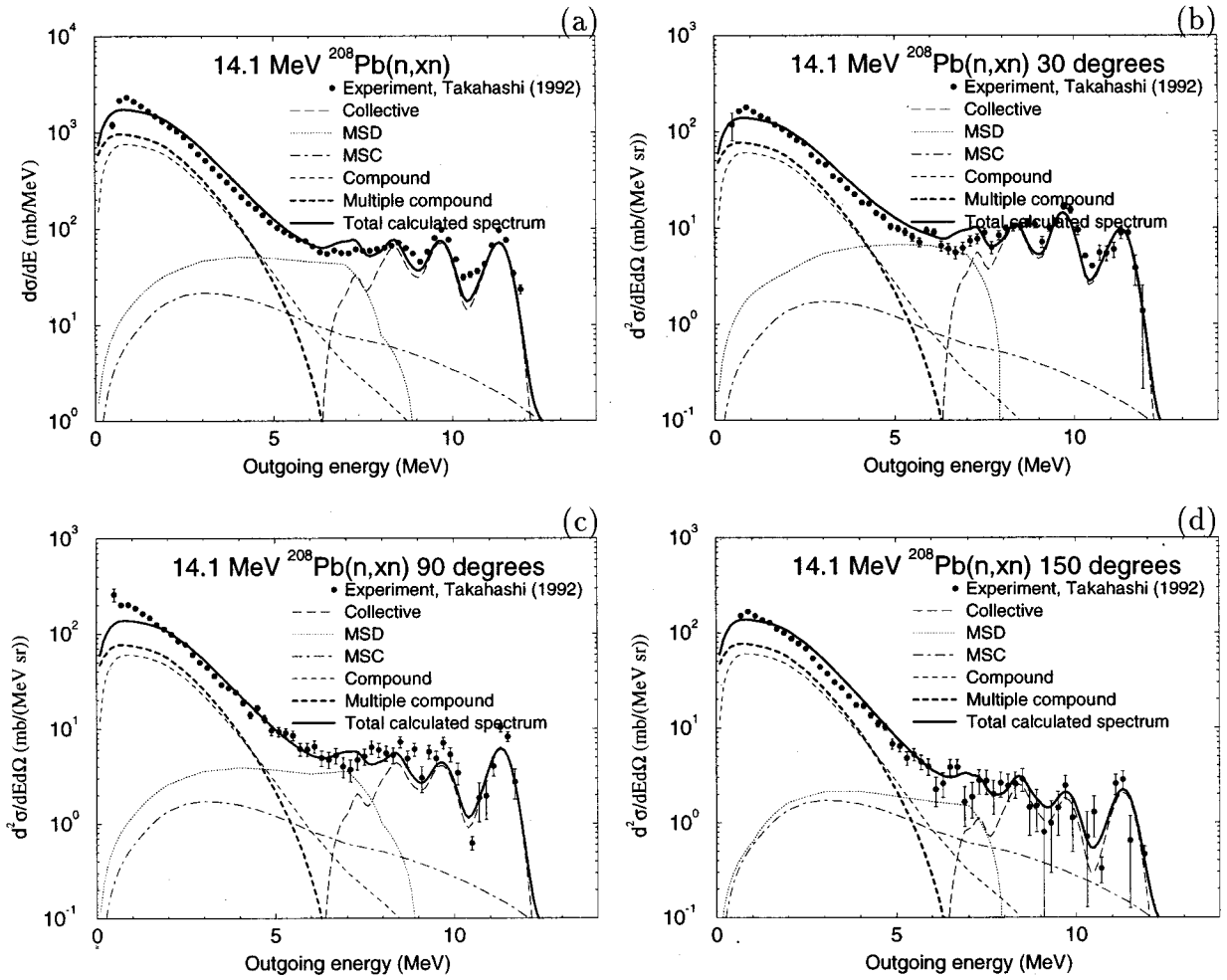

FIG. 7. Comparison of fully microscopical calculations with experimental data [66] for the ^{208}Pb(n,xn) reaction at 14.1 MeV: (a) angle-integrated spectrum, (b) 30°, (c) 60°, and (d) 150°.

ence in predictive power is manifest mostly for the most forward and backward angles. At backward angles, the intranuclear cascade (INC) model in HETC underpredicts the emission spectra. This is because quantum mechanical diffraction and refraction effects, automatically included in the MSD theory (but not in INC), enhance the back-angle emission cross sections. In the semiclassical INC model nucleon-nucleon scattering off a stationary nucleon cannot result in scattering beyond 90°, though Fermi-motion, semiclassical treatments of refraction, and multistep scatterings, will broaden the angular distribution to higher angles, though still the differential back-angle cross sections are too low. Additionally, the INC model tends to overestimate the quasifree scattering peak at the very forward angles for this incident energy [73].

For all reactions below 60 MeV, we have varied the relevant component of the strength of the effective interaction until the calculated results were in optimal agreement with the experimental data. For reactions above 60 MeV, we only specified the ratio $V_{\pi\pi}/V_{\pi\nu}$. We have consistently taken a ratio of 1 for these energies, which essentially makes our approach parameter-free for $E>60$ MeV. This value does not coincide with Austin's ratio of 3.4 but does, on the other hand, follow directly from phenomenology. Kalend *et al.*

TABLE III. Optical potentials used for the reactions studied in this paper [61–65].

Nuclide	Neutrons	Protons
^{27}Al	$E<90$ MeV: Walter-Guss	$E<50$ MeV: Becchetti-Greenlees
	$E>90$ MeV: Madland	$E>50$ MeV: Madland
^{56}Fe	$E<80$ MeV: Pedroni	$E<50$ MeV: Becchetti-Greenlees
	$E>80$ MeV: Madland	$E>50$ MeV: Madland
^{90}Zr	$E<90$ MeV: Walter-Guss	$E<20$ MeV: Becchetti-Greenlees
	$E>90$ MeV: Madland	$E>20$ MeV: Menet
^{208}Pb	$E<200$ MeV: Johnson	$E<200$ MeV: Liegeois-Delaroche

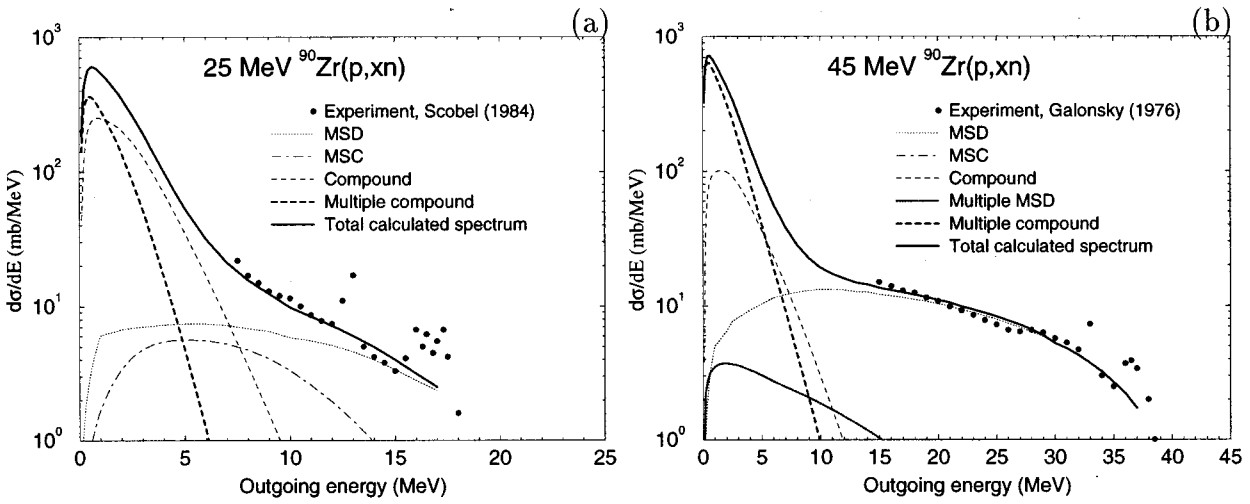

FIG. 8. Angle-integrated spectra for ^{90}Zr (p,xn). Comparison of fully microscopical calculations with experimental data: (a) 25 MeV [67], (b) 45 MeV [68].

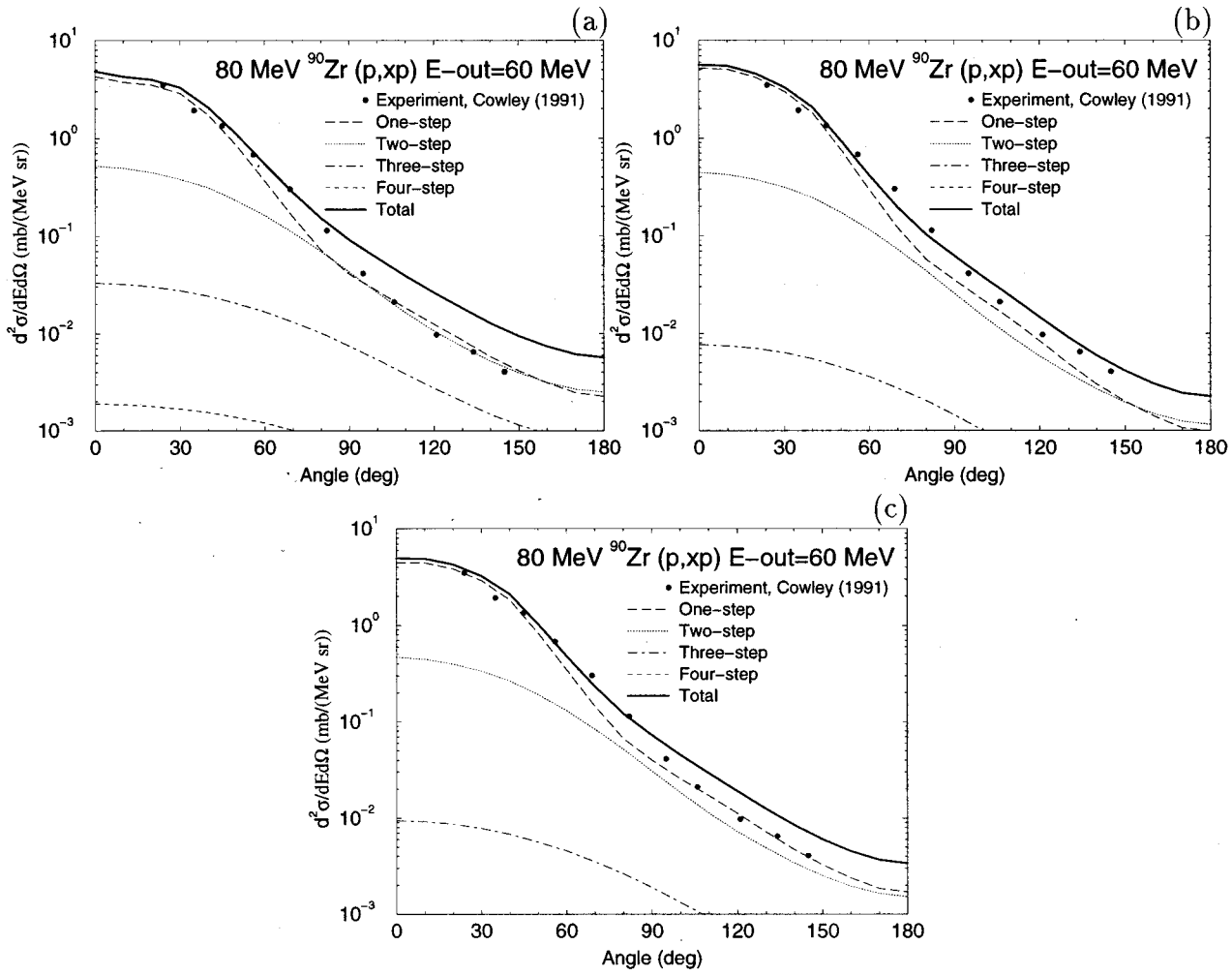

FIG. 9. Comparison of calculated double-differential cross sections, using the potentials of Madland and Becchetti-Greenlees, with experimental data for 80 MeV ^{90}Zr (p,xp) [36] at an outgoing energy of 60 MeV: (a) fully microscopic, (b) state density-based calculations with a constant spin cutoff factor (2.21), and (c) with an energy-dependent spin cutoff factor (5.14).

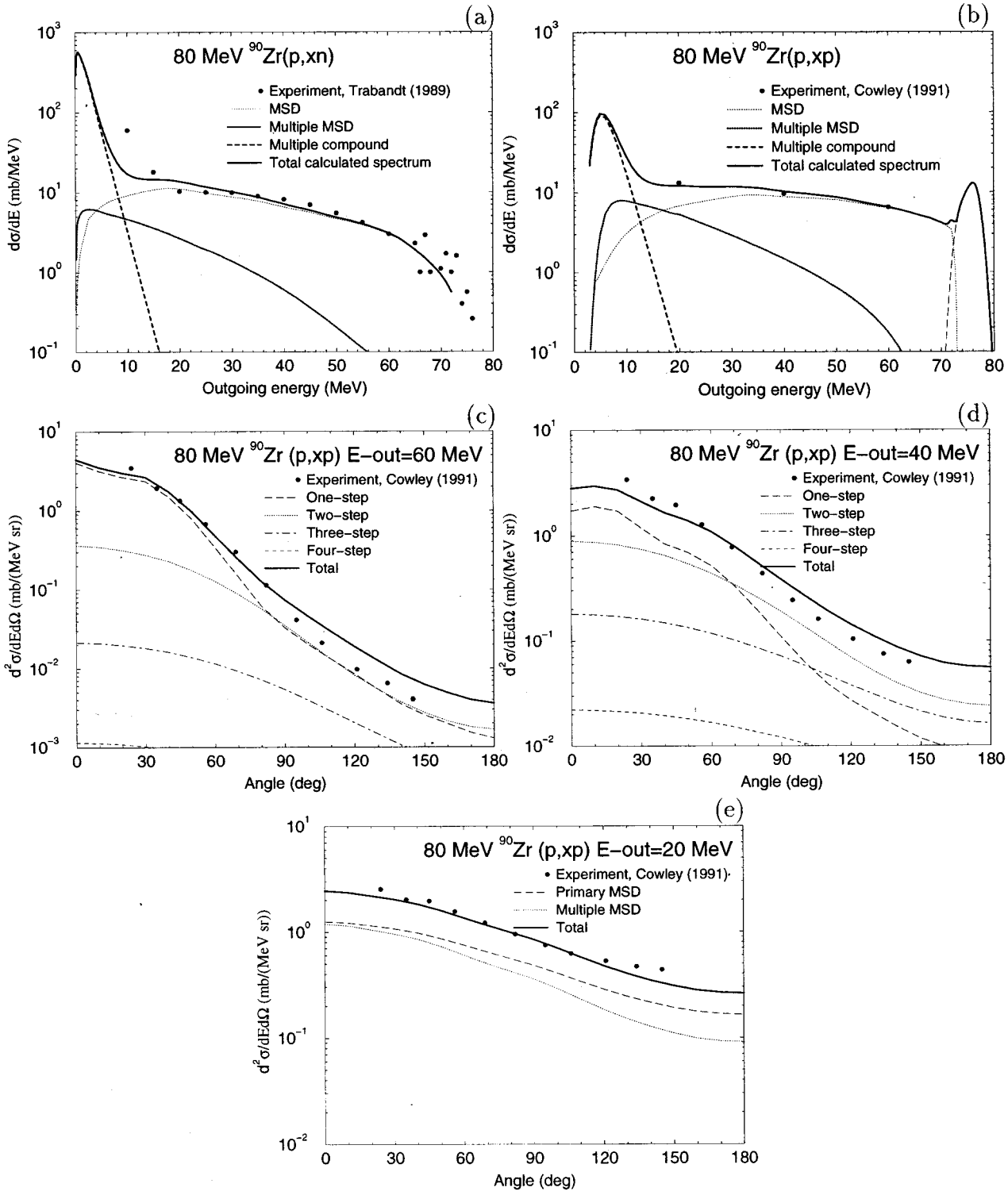

FIG. 10. Comparison of fully microscopical calculations, with the potentials of Menet and Becchetti-Greenlees, with experimental data for 80 MeV protons on ^{90}Zr: (a) angle-integrated (p,xn) cross section [69], (b) angle-integrated (p,xp) cross section. Double-differential (p,xp) cross section at outgoing energies of (c) 60 MeV, (d) 40 MeV, and (e) 20 MeV.

[70] have made the interesting observation that for proton-induced reactions around 90 MeV the emission spectra in the pre-equilibrium regime for outgoing protons are about twice as large as that of outgoing neutrons. Figures 10(a) and 10(b), and 11 confirm this trend. For the highest outgoing energies, only one-step direct cross sections contribute and we can infer the following ratio from Eqs. (2.15) and (2.16):

$$\frac{\sigma_{pp}}{\sigma_{pn}}=\frac{g_\pi^2\sigma_{pp}^{\mathrm{DWBA}}(V_{\pi\pi})+g_\nu^2\sigma_{pp}^{\mathrm{DWBA}}(V_{\pi\nu})}{g_\pi g_\nu\sigma_{pn}^{\mathrm{DWBA}}(V_{\pi\nu})}$$

$$\approx\frac{Z^2V_{\pi\pi}^2+N^2V_{\pi\nu}^2}{ZNV_{\pi\nu}^2}=\frac{V_{\pi\pi}^2+V_{\pi\nu}^2}{V_{\pi\nu}^2}\quad\text{if } Z=N. \quad (7.2)$$

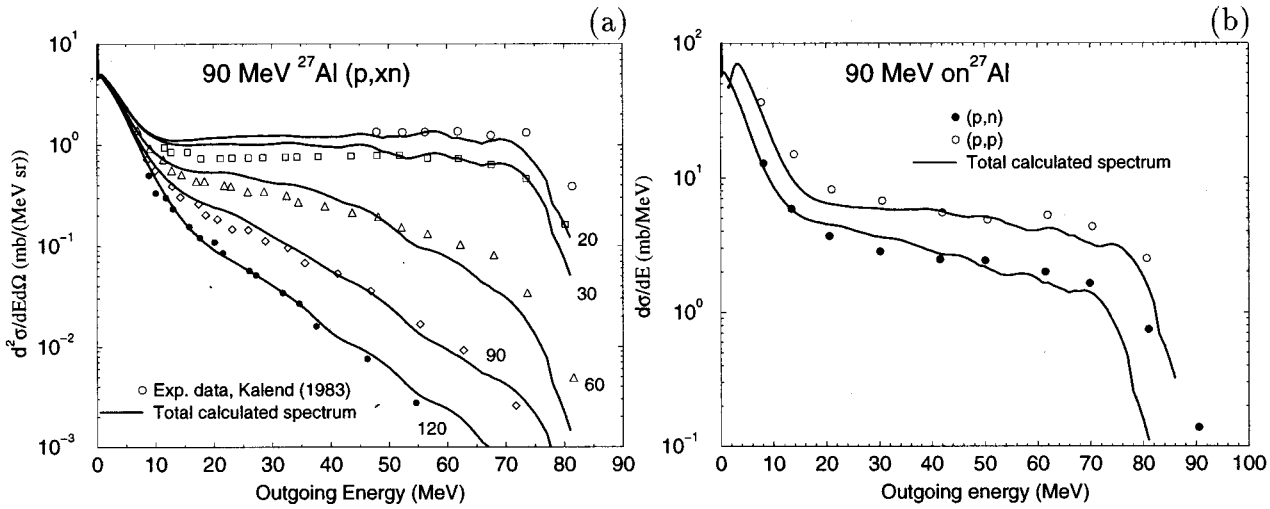

FIG. 11. Comparison of fully microscopical calculations with experimental data [70] for 90 MeV protons on ^{27}Al: (a) double-differential (p,xn) cross section, (b) angle-integrated (p,xp) cross section.

For $Z=N$, we find the 2:1 ratio only if $V_{\pi\pi}=V_{\pi\nu}$. If we would use Austin's ratio, i.e., $V_{\pi\nu}\sim 3.4V_{\pi\pi}$, we find a ratio of about 1:1 which is not observed in the measurements. Hence, the difference between our parametrization and that of Austin must stem from aspects that are not yet taken into account in this paper, such as the role of isospin conservation within MSD reactions.

However, our finding that measured emission spectra are best reproduced when a $V_{\pi\pi}/V_{\pi\nu}$ ratio of 1 is used is not unique. Kalend's work [70] also implicitly contains this conclusion. They estimate the ratio of emitted fast protons to neutrons using quasifree scattering arguments, and obtain approximately $(\sigma_{pp}+\sigma_{pn})/\sigma_{pn}$ in the $N=Z$ limit. This only gives a ratio of two when $\sigma_{pp}\approx\sigma_{pn}$. Also, in Kalbach's recent exciton model analysis [74], a ratio of 1 was found to best reproduce experimental data.

In Table II the extracted values are presented. We used the values for $V_{\pi\nu}$ to obtain the following, incident energy-dependent, expression:

$$V_{\pi\nu}=31.8\exp\left(-\frac{0.20}{31.8}E\right), \tag{7.3}$$

which is similar to the simpler one-component V_0 results [1], see Sec. V D. This energy dependence for the strength of the effective interaction is included in MINGUS, so that for lower incident energies that appear for the higher steps, consistent values are taken.

VIII. CONCLUSIONS AND FUTURE WORK

We have presented a new model for the computation of multistep direct reactions. The theoretical improvement consists of an extension of the MSD formalism to a model that distinguishes between protons and neutrons for both the leading particle and the excited particles and holes for all orders of scattering. Our formalism enables both completely microscopical calculations, in which all particle-hole states as predicted by the shell model are included, and an approximate approach using partial state densities and averaged DWBA cross sections. We have adopted the FKK model for the second and higher steps. In the two-component approach, the attractive convolution structure of the multistep cross section remains present, though an extra summation over intermediate neutrons and protons appears. Particle-hole states are generated with a spherical Nilsson model and each individual $1p1h$ state is spread over the energy spectrum using a Gaussian distribution. For fully microscopic calculations, these states are then adopted for our MSD model. When state densities are used, the distance between the energies of the particle-hole states and the considered excitation energy is appropriately taken into account in the DWBA average. This approach is more realistic than the conventional arithmetic average used in the literature. Furthermore, our analysis indicates that previous works have overestimated the accessible state densities by a factor of 2 since non-normal parity states cannot be excited using a spin-independent interaction. This overestimate influences the value of the residual interaction strength extracted in previous works.

Inconsistencies in the multistep cross section expansion, as they appear in one-component approaches, are resolved by using the two-component formalism. For completeness, correction factors to be applied to the older one-component results are presented, to approximate the full two-component theory, though we stress that such factors need not be used if the two-component theory is adopted for calculations. All complementary reaction models, namely, direct, MSC, and compound are included. Comparisons of MINGUS calculations with measurements illustrate the sensitivity of the results to the optical models and the shape of the spin distribution. Allowing ourselves the adjustment of one parameter, the (ratio of the) strength of the effective interaction, we obtain a globally good description of experimental double-differential continuum spectra.

Although our method removes several existing uncertainties within MSD approaches, we appreciate that many aspects still need to be explored.

Spin transfer reactions. We have only included normal parity states in our analysis, in line with our choice of a simple central form for the effective nucleon-nucleon inter-

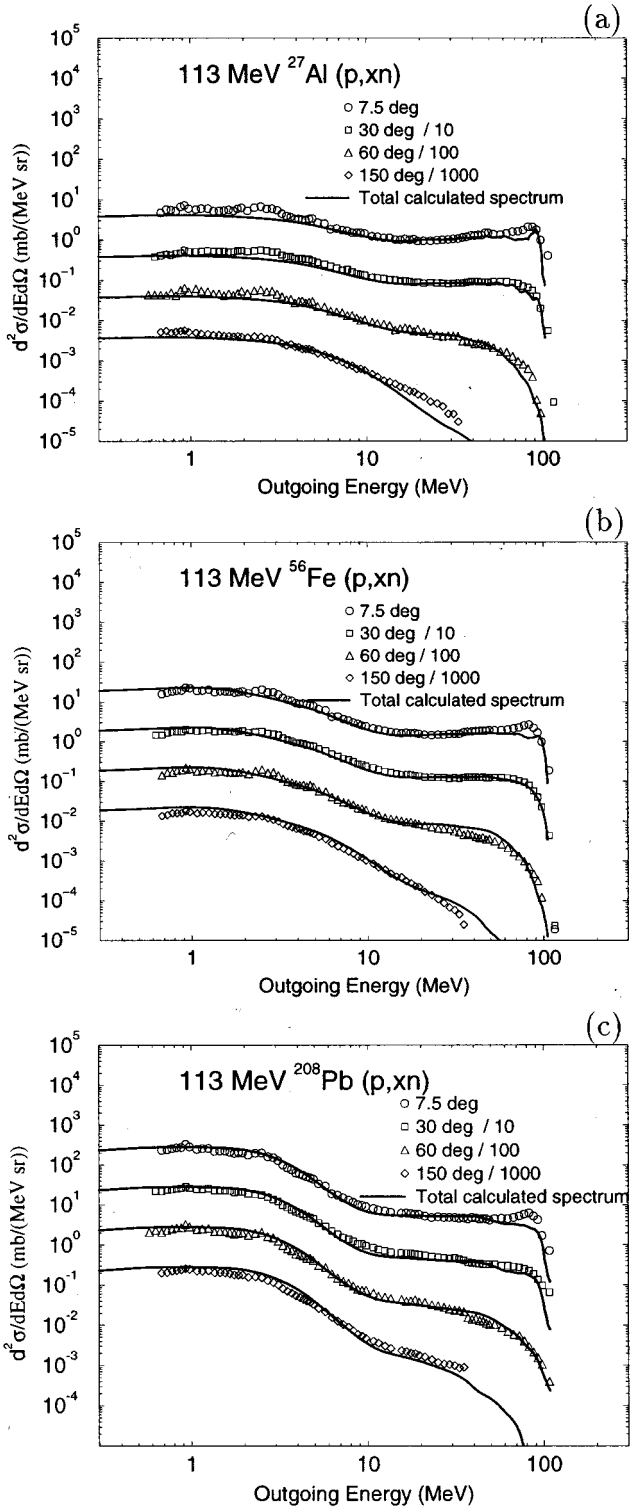

FIG. 12. Comparison of fully microscopical calculations with experimental data [72] for 113 MeV (p,xn) double-differential cross sections for (a) Al, (b) Fe, and (c) Pb.

action. An obvious extension is to employ the full expansion of $\mathcal{V}$, including noncentral, imaginary, and spin-orbit terms and thereby also the associated DWBA transitions to non-normal parity states. Raynal's DWBA91 code can be included in our system for such calculations. This aspect is intimately connected with analyzing powers in the continuum, and our MSD approach may shed new light on continuum polarization phenomena. An adequate analysis will require realistic spin-orbit terms in both the effective interaction and the optical potential. Additional further work is needed to address problems encountered in DWBA calculations for particle-hole states with high spin [76].

The Tamura-Udagawa-Lenske (TUL) *model*. From the theoretical point of view, the multistep method described in this paper can be easily modified to calculate the full multistep matrix element, including all two-component aspects. This would enable a microscopic validation of the TUL model (either with or without the use of state densities). With regard to the MSD literature of the past decade, the TUL model is perhaps less controversial than the FKK model. The randomness of the distribution amplitudes [Eq. (2.5)] is the only basic statistical assumption underlying the TUL theory for the higher steps, and has been verified independently in nuclear structure studies [11]. A restrictive practical aspect of the approach of Ref. [4], the use of l-independent *macroscopic* form factors for all DWBA transitions, has been resolved in this paper for the first step. We have not yet investigated whether microscopic calculations for the higher steps are really feasible with regard to computer power. Monte Carlo techniques for the sampling of particle-hole states may be necessary.

Unbound 1p1h states. Recently, the code ECIS has been extended to include the possibility for calculating transitions to unbound particle-hole states. The physical meaning of these calculations and their application in MSD reaction theory is presently under study. Inclusion of these unbound states may lead to more realistic MSD results, especially for multiple MSD emission when more than one continuum particle is present.

Adequate optical potentials. Most calculations in this paper were based on global optical model parametrizations and we have confirmed the sensitivity of the MSD results on the optical model parameters. Optical models especially tailored to the nucleus under consideration would at least reduce another uncertainty of quantum-mechanical preequilibrium calculations. Potentials constructed from microscopic information, such as provided by Jeukenne, Lejeune, and Mahaux [75], may be most preferable.

Multiple pre-equilibrium emission. The present available method is, although practically very efficient, theoretically not yet at a satisfactory level. The recent work of Arbanas [59] provides an important theoretical advance in this area.

Realistic single-particle level schemes and level densities. Although the equidistant spacing model that leads to the simple analytical expression (2.18) has been quite successful for the analysis of preequilibrium spectra, we feel that realistic single-particle level schemes would provide the MSD method with a more physical basis. Both for a fully microscopic approach and for an approach using state densities, level schemes built from fundamental nucleon-nucleon interactions should be preferred.

Ideally, an MSD analysis should include the most sophisticated ingredients from other independent nuclear structure/reaction studies, so that uncertainties in the cross section calculations can be reduced, facilitating a better test of the underlying quantum statistical assumptions. In the present context, this means use of a level density prescription based on a realistic microscopical level scheme, as much discrete level information as possible, high-quality optical models

and a state-of-the-art prescription of the nucleon-nucleon interaction.

ACKNOWLEDGMENTS

We wish to thank J. Raynal for valuable discussions concerning the use of his ECIS code and C. Kalbach for performing the isospin-dependent exciton model calculations. We also gratefully acknowledge useful conversations with O. Bersillon, J.-P. Delaroche, F. Dietrich, S. Grimes, A. Kerman, A. Marcinkowski, Y. Watanabe, and P. Young. A. Koning wishes to thank Los Alamos National Laboratory for the hospitality during his stay.

[1] E. Gadioli and P.E. Hodgson, *Pre-equilibrium Reactions* (Clarendon, Oxford, 1992).
[2] R. Bonetti, M.B. Chadwick, P.E. Hodgson, B.V. Carlson, and M.S. Hussein, Phys. Rep. **202**, 171 (1991).
[3] R. Bonetti, A.J. Koning, J.M. Akkermans, and P.E. Hodgson, Phys. Rep. **247**, 1 (1994).
[4] T. Tamura, T. Udagawa, and Lenske, Phys. Rev. C **26**, 379 (1982).
[5] R. Bonetti, L. Colli Milazzo, A. De Rosa, G. Inglima, E. Perillo, M. Sandoli, and F. Shanin, Phys. Rev. C **21**, 816 (1980).
[6] R. Bonetti, M. Camnasio, L.C. Milazzo, and P.E. Hodgson, Phys. Rev. C **24**, 71 (1981).
[7] *Multistep Direct Reactions*, Proceedings of the Conference Faure, South Africa, edited by R.H. Lemmer (World Scientific, Singapore, 1992).
[8] H. Feshbach, A. Kerman, and S. Koonin, Ann. Phys. (N.Y.) **125**, 429 (1980).
[9] C. Kalbach, Phys. Rev. C **37**, 2350 (1988).
[10] H. Nishioka, H.A. Weidenmüller, and S. Yoshida, Ann. Phys. (N.Y.) **183**, 166 (1988).
[11] A.J. Koning and J.M. Akkermans, Ann. Phys. (N.Y.) **208**, 216 (1991).
[12] A.J. Koning and J.M. Akkermans, Phys. Rev. C **47**, 724 (1993).
[13] P. Demetriou, P.E. Hodgson, A. Marcinkowski, and Y. Watanabe, J. Phys. G **22**, 629 (1996).
[14] H. Nishioka and H.A. Weidenmüller, Phys. Lett. B **203**, 1 (1988).
[15] F.C. Williams, Nucl. Phys. **A166**, 231 (1971).
[16] H. Feshbach, P.E. Hodgson, A.J. Koning, and J.M. Akkermans, in *Multistep Direct Reactions* [7].
[17] M.B. Chadwick, P.G. Young, and F.S. Dietrich, *Intermediate Energy Nuclear Data: Models and Codes*, Issy-les-Moulineaux, France, 1994 (unpublished), p. 67.
[18] H. Feshbach, Ann. Phys. (N.Y.) **159**, 150 (1985).
[19] E. Betak and J. Dobes, Z. Phys. A **279**, 319 (1976).
[20] H. Gruppelaar, ''IAEA Advisory Group Meeting on Basic and Applied Problems on Nuclear Level Densities,'' Brookhaven National Laboratory report, 1983 (unpublished), p. 143.
[21] A. Bohr and B.R. Mottelson, *Nuclear Deformations*, Vol. 2 of *Nuclear Structure* (Benjamin, Reading, MA, 1975), p. 219.
[22] P.J. Brussaard and P.W.M. Glaudemans, *Shell Model Applications in Nuclear Spectroscopy* (North-Holland, Amsterdam, 1977).
[23] P.A. Seeger and W.M. Howard, Nucl. Phys. **A238**, 491 (1975).
[24] M.B. Johnson, L.W. Owens, and G.R. Satchler, Phys. Rev. **142**, 748 (1966).
[25] M.B. Chadwick, P.G. Young, P. Oblozinsky, and A. Marcinkowski, Phys. Rev. C **49**, R2885 (1994).
[26] J. Raynal, ''Notes on ECIS94,'' CEA Saclay Report No. CEA-N-2772, 1994 (unpublished).
[27] J. Raynal (private communication).
[28] J. Dobes and E. Betak, Z. Phys. A **310**, 329 (1983).
[29] C. Kalbach, Phys. Rev. C **33**, 818 (1986).
[30] M. Herman and G. Reffo, Phys. Rev. C **39**, 1269 (1989).
[31] Y. Watanabe, A. Aoto, H. Kashimoto, S. Chiba, T. Fukahori, K. Hasegawa, M. Mizumoto, S. Meigo, M. Sugimoto, Y. Yamanouti, N. Koori, M.B. Chadwick, and P.E. Hodgson, Phys. Rev. C **51**, 1891 (1995).
[32] M.B. Chadwick, P.G. Young, D.C. George, and Y. Watanabe, Phys. Rev. C **50**, 996 (1994).
[33] A.J. Koning, O. Bersillon and J.-P. Delaroche, *Intermediate Energy Nuclear Data: Models and Codes* [17], p. 87.
[34] W.A. Richter, A.A. Cowley, G.C. Hillhouse, J.A. Stander, J.W. Koen, S.Y. Steyn, R. Lindsay, P.E. Julies, J.J. Lawrie, J.V. Pilcher, and P.E. Hodgson, Phys. Rev. C **49**, 1001 (1994).
[35] M. Herman and G. Reffo, *OECD Meeting on Nuclear Level Densities*, Bologna, Italy, 1989 (unpublished), p. 103.
[36] A.A. Cowley, A. van Kent, J.J. Lawrie, S.V. Förtsch, D.M. Whittal, J.V. Pilcher, F.D. Smit, W.A. Richter, R. Lindsay, I.J. van Heerden, R. Bonetti, and P.E. Hodgson, Phys. Rev. C **43**, 678 (1991).
[37] S. M. Austin, *The (p,n) Reaction and the Nucleon-Nucleon Force*, Telluride, Colorado, 1979 (Plenum, New York, 1979), p. 203.
[38] J. Raynal (private communication) (author of ECIS95 and DWBA91). Most previous FKK analyses have used DWUCK instead of ECIS95. It appears that MSD practitioners have omitted a factor of $2j_h+1$ in DWBA calculations with DWUCK. The correction factors that we would apply on the old one-component calculations are then approximately cancelled by an erroneous normalization in the DWBA calculation.
[39] C. Kalbach, Phys. Rev. C **30**, 1310 (1984).
[40] C. Kalbach, in *Proceedings of a Specialists' Meeting on Pre-equilibrium Reactions*, Semmering, Austria, 1988, edited by B. Strohmaier (OECD, Paris, 1988), p. 197.
[41] C. Kalbach, in *Proceedings of International Symposium on Pre-Equilibrium Reactions*, Smolenice, Slovakia, October, 1995 [Acta Phys. Slov. **45**, 685 (1995)].
[42] S.M. Grimes, Phys. Rev. C **46**, 1064 (1992); S.M. Grimes, J.D. Anderson, A.K. Kerman, and C. Wong, *ibid.* **5**, 85 (1972).
[43] Y. Watanabe *et al.*, Phys. Rev. C **36**, 1325 (1990).
[44] Y. Watanabe, in *Proceedings of International Symposium on Pre-Equilibrium Reactions*, Smolenice, Slovakia, 1995 [41].
[45] C. Kalbach (private communication).
[46] R.L. Feinstein, Ann. Phys. (N.Y.) **107**, 222 (1977).
[47] A.J. Koning, O. Bersillon, and J.-P. Delaroche, *International Conference on Nuclear Data for Science and Technology*, Gatlinburg, Tennessee, 1994 (unpublished), p. 1072.

[48] A. Marcinkowski, B. Marianski, P. Demetriou, and P.E. Hodgson, Phys. Rev. C **52**, 2021 (1995).
[49] P. Demetriou, A. Marcinkowski, and P.E. Hodgson, Nucl. Phys. **A596**, 67 (1996).
[50] M.B. Chadwick and P.G. Young, Phys. Rev. C **47**, 2255 (1993).
[51] P. Oblozinsky, Nucl. Phys. **A453**, 127 (1986).
[52] A. Marcinkowski, J. Rapaport, R.W. Finlay, C. Brient, M. Herman, and M.B. Chadwick, Nucl. Phys. **A561**, 387 (1993).
[53] A. Gilbert and A.G.W. Cameron, Can. J. Phys. **43**, 1446 (1965).
[54] A.V. Ignatyuk, G.N. Smirenkin, and A.S. Tishin, Sov. J. Nucl. Phys. **21**, 255 (1975).
[55] J.P. Brancazio and A.G.W. Cameron, Can. J. Phys. **47**, 1029 (1969).
[56] M.B. Chadwick, Los Alamos National Laboratory Report No. LA-UR-92-2346, 1992 (unpublished).
[57] M. Blann and H. Vonach, Phys. Rev. C **28**, 1475 (1983).
[58] L.I. Schiff, *Quantum Mechanics* (McGraw-Hill, New York, 1968).
[59] G. Arbanas, Ph.D. thesis, Massachusetts Institute of Technology, 1995.
[60] R. Michel and P. Nagel, ''International Dode Comparison for Intermediate Energy Activation Yields,'' NEA Report No. NSC/DOC(97)-1 (1997).
[61] D.G. Madland, in *Proceedings of a Specialists' Meeting on Preequilibrium Reactions* [40], p. 103; International Atomic Energy Agency Report No. IAEA-TECDOC-483, 1988 (unpublished), p. 80.
[62] R.L. Walter and P.P. Guss, in *Nuclear Data for Basic and Applied Science*, Santa Fe, New Mexico, 1985, edited by P.G. Young (Gordon and Breach, New York, 1986), p. 1079.
[63] F.D. Becchetti and G.W. Greenlees, Phys. Rev. C **182**, 1190 (1969).
[64] J.J.H. Menet, E.E. Gross, J.J. Malanify, and A. Zucker, Phys. Rev. C **4**, 1114 (1971).
[65] R.S. Pedroni, C.R. Howell, G.M. Honoré, H.G. Pfutzner, R.C. Byrd, and R.L. Walter, Phys. Rev. C **38**, 2052 (1988).
[66] A. Takahashi, M. Gotoh, Y. Sasaki, and H. Sugimoto, OKTAVIAN Report No. A-92-01, 1992 (unpublished).
[67] W. Scobel, M. Blann, T.T. Komoto, M. Trabandt, S.M. Grimes, L.F. Hansen, C. Wong, and B.A. Pohl, Phys. Rev. C **30**, 1480 (1984).
[68] A. Galonsky, R.R Doering, D.M. Patterson, and H.W. Bertini, Phys. Rev. C **14**, 748 (1976).
[69] M. Trabandt, W. Scobel, M. Blann, B.A. Pohl, R.C. Byrd, C.C. Foster, R. Bonetti, and S.M. Grimes, Phys. Rev. C **39**, 452 (1989).
[70] A.M. Kalend, B.D. Anderson, A.R. Baldwin, R. Madey, J.W. Watson, C.C. Chang, H.D. Holmgren, R.W. Koontz, J.R. Wu, and H. Machner, Phys. Rev. C **28**, 105 (1983).
[71] M.B. Chadwick and P. Oblozinsky, Phys. Rev. C **50**, 2490 (1994).
[72] M.M. Meier, D.A. Clark, C.A. Goulding, J.B. McClelland, G.L. Morgan, and C.E. Moss, Nucl. Sci. Eng. **102**, 310 (1989).
[73] M. Blann, H. Gruppelaar, P. Nagel, and J. Rodens, *Intermediate Energy Code Intercomparison*, Nuclear Energy Agency (OECD, Paris, 1994).
[74] C. Kalbach, J. Phys. G **21**, 1519 (1995).
[75] J.-P. Jeukenne, A. Lejeune, and C. Mahaux, Phys. Rev. C **16**, 80 (1977).
[76] F. Dietrich (private communication).